Polarized-x-ray-absorption studies of graphite intercalated-bromine compounds

J. L. Feldman, W. T. Elam, A. C. Ehrlich, E. F. Skelton, and D. D. Dominguez
Naval Research Laboratory, Washington, D.C. 20375-5000

D. D. L. Chung
Department of Metallurgical Engineering and Materials Science, Carnegie-Mellon University, Pittsburgh, Pennsylvania 15213

F. W. Lytle
The Boeing Company, Seattle, Washington 98124

(Received 23 December 1985; revised manuscript received 10 March 1986)

Details of both results and data analysis are given in the case of our polarized-x-ray-absorption experiments, using synchrotron radiation, on highly oriented pyrolytic graphite (HOPG)—based and graphite-fiber-based residual-bromine intercalation compounds. The effective angle which nearest-neighbor Br pairs make with crystallite graphite planes in some of these compounds, which was stated to be $\sim 20°$ in an earlier article, is shown to be $16° \pm 4°$—both Br-Br extended x-ray-absorption fine structure (EXAFS) and white-line features of the data are the basis of this result. We have also found that, whereas spherical averages of the areas under white-line spectra are independent of the choice of the material among all samples studied (including Br_2 vapor), differences in similarly spherically averaged Br-Br EXAFS amplitudes are evident, especially between Br_2 vapor and Br-graphite samples. We show that the latter differences which correspond to a coordination number less than one in Br-graphite are not due to either Gaussian or non-Gaussian (up to k^4 terms) Debye-Waller effects. In addition, we discuss the extraction of Br-C EXAFS and present results of model calculations of Br-C EXAFS, where several different structural models for the Br sites are considered. We also discuss thermal effects and their relation to known Br sublattice phase-transition behavior, based on our measurements at room temperature, 360 K, and 400 K.

I. INTRODUCTION

We have discussed the Br K-edge x-ray-absorption spectra of certain graphite-bromine intercalation compounds (GIC-Br) in recent abbreviated publications.[1,2] In this paper, a much more complete and detailed study of GIC-Br is presented. The relation of these results to previously observed phase transitions[3] in these compounds also will be presented here.

For purposes of determining the short-range structural order in GIC-Br, it is necessary to make extended x-ray-absorption fine structure (EXAFS) measurements because of difficulties in unambiguously analyzing x-ray diffraction data. This is due to the lack of long-range correlation, along the c axis, of the in-plane intercalate structure. We have used highly oriented pyrolytic graphite (HOPG) and pitch-based graphite fibers and believe the analysis of the results for these materials to be generally more conclusive (although not entirely unambiguous) than that for Grafoil, whose EXAFS properties have been studied,[4] because there exists a more orderly arrangement of the graphite planes in the former materials than in the latter one.

One rather interesting conclusion drawn from this work, although the same result was conjectured independently for the case of concentrated compounds,[5] is that nearest-neighbor Br pairs are oriented at a finite angle to the neighboring graphitic planes. The evidence for this will be given here in detail and the accuracy with which we have determined this angle will be discussed.

Several structural transitions of the intercalate layers of GIC-Br have been discovered.[3,5–8] Particular to our study, x-ray diffraction studies[3,5,8] show that commensurate-incommensurate (C-I) and melting transitions occur in HOPG-based, as well as single-crystal-graphite—based GIC-Br. These latter transitions also occur for a range of Br concentrations that includes the concentrations of our samples which are ~ 2–5 at.%. The melting transition temperature is 373 K and the C-I transition temperature, which is dependent on stage,[8] or concentration, is 350 K for residue compounds (which we study here). As further evidence of a melting transition in GIC-Br's, the Raman intensity of a resonant Raman mode associated with the bromine sublattice[9,10] was found to vanish above $T = 380$ K (Ref. 11). (We note, however, that the samples used in our study were not investigated by either x-ray diffraction measurements or Raman measurements.) Clearly it is also interesting to know if there is any change in Br-Br and Br-C EXAFS corresponding to these transitions. We have therefore included measurements at room temperature (300), 360, and 400 K in our studies; at these temperatures desorbed HOPG-based GIC-Br is known to be in a commensurate, incommensurate, and melted state, respectively.

The amplitude of the Br-Br EXAFS has been discussed for several compounds involving Br, such as compounds with $(SN)_x$ (Ref. 12) and polyacetylene[13] in addition to Br-graphite.[1,2,4] Generally, the amplitude is found to be less than expected on the basis of Br_2 vapor results. We

have suggested[2] that at least in the case of Br-graphite this amplitude effect is "electronic" in origin. One possible "structural" explanation that was not considered previously in the case of these materials, namely, a non-Gaussian Debye-Waller factor, is considered here and found to be insufficient.

We review the standard EXAFS expression in order to point out the approximations upon which our analysis is based. We write the single-particle-scattering EXAFS formula as

$$\chi \equiv \frac{\mu-\mu_0}{\mu_0} = \frac{3NF(k)}{kr^2}\langle\cos^2\theta\rangle e^{-2k^2\sigma^2}e^{-2r/l} \times \sin[2kr+\phi(k)] \quad (1)$$

for a particular atom-pair type, interatomic distance r, and orientation of the x-ray polarization with respect to the sample. Also, N is the coordination number, σ is a root-mean-square relative displacement, l is an electronic inelastic mean free path, θ is the angle made by the x-ray polarization $\hat{\epsilon}$ and one of the interatomic vectors $\mathbf{r}$, k is the outgoing electron wave number, and $F(k)$ and $\phi(k)$ are the appropriate electronic amplitude factor (which may also include certain multielectron effects) and phase function, respectively. For intercalated HOPG and graphite fibers the quantity $\langle\cos^2\theta\rangle$, which represents an average over all bonds in the sample, depends explicitly on $\hat{\epsilon}$, and on an effective angle α_{eff} between an atom pair and the nearby graphite planes (see Ref. 1 for the specific relations). It is presumed that σ, F, and l are independent of both the location of a particular atom pair and the sample orientation with respect to $\hat{\epsilon}$. It is conceivable that F and l depend on sample orientation and that σ, F, and l depend on atom-pair location, but there is no *a priori* information on this. Further, it is simple to show that in the case of a variety of coordination numbers Eq. (1) is valid, but with N replaced by the average coordination number.

This paper is organized as follows: In Sec. II the sample preparations are discussed; in Sec. III, the details of the data analysis are discussed; in Sec. IV, results and analysis for Br_2 vapor are given; in Sec. V, checks on the polarization of the x-ray beam based on our absorption measurements are described; in Sec. VI, results for nearest-neighbor Br-Br EXAFS in GIC-Br materials are compared; in Sec. VII, white-line spectral results are compared; in Sec. VIII, evidence is given of Br-C EXAFS as well as of Br-Br EXAFS corresponding to weakly bonded, non-nearest-neighbor atoms. In addition, some results illustrating the accuracy of the data analysis and polarization assumptions are contained in Secs. VII and VIII. Details of model calculations of Br-C EXAFS are presented in Sec. IX, possible non-Gaussian Debye-Waller effects in Br-Br EXAFS are discussed in Sec. X, and a comparison with the EXAFS measurements of Heald and Stern[4] on Br *adsorbed* Grafoil is given in Sec. XI. Finally, a summary is given in Sec. XII.

II. SAMPLE PREPARATION AND EXPERIMENTAL DETAILS AND UNCERTAINTIES

In previous x-ray diffraction studies, it was found that whereas the intercalate two-dimensional unit cell, corresponding to the commensurate phase, is invariant with respect to sample preparation, positions within the unit cell are not. In this work, samples with two types of preparation are studied: two TP4104B pitch-based graphite-fiber samples and one HOPG sample were obtained by intercalating in Br_2 vapor at room temperature until fully intercalated (stage 2) and then desorbing in vacuum at room temperature for several hours. Furthermore, it was this HOPG sample and one of these two fiber samples that were studied as a function of temperature. (Unfortunately our limited beam time prohibited measurements of our other samples at elevated temperatures.) In addition, an HOPG sample which was prepared from different virgin HOPG than was the other sample and which was intercalated in liquid at room temperature until fully intercalated (stage 2) and desorbed in air at 100 °C for $\frac{1}{2}$ h was studied at room temperature. We denote the former HOPG-based sample as HOPGv and the latter as HOPGl. The great advantage of working with samples that have been intercalated and then deintercalated, known as residue intercalation compounds, is that they are known to be highly stable. We note here that diffraction measurements, both our own and others, on residue samples of pitch-based fiber GIC-Br's have failed to show evidence of intercalation although such evidence has been obtained for fiber GIC-ICl (Ref. 14). Thus, it is possible that the fibers are not truly intercalated. As we will see, a result of this work is that there is a very similar orientation, with respect to the graphitic planes, of nearest-neighbor bromine pairs in fiber- and HOPG-based samples. This implies that the bromine is at least adsorbed onto graphite crystallites in the fibers, if not truly intercalated. In addition, a somewhat weaker argument for true intercalation on the basis of our Br-C EXAFS will be made later in the paper. We have also observed a dramatic increase in electrical conductivity upon "intercalation" of the fibers, but this too is not a definitive proof of intercalation.

The quantity $\Delta\mu x$, i.e., the jump in μx at the main edge, was found to be 0.22 and 0.43 for the fiber samples 1 and 2, respectively, 0.22 and 1.42 for HOPGv and HOPGl, respectively, and 0.62 for Br_2 vapor, where these values for Br graphite correspond to the beam directed perpendicularly to the fiber axis and, in the case of the HOPG samples, to the graphite planes. The HOPGv sample was constructed by placing one layer of ≈ 1 mm squares of HOPGv of thickness ≈ 0.05 mm flat on a piece of Mylar, whereas the HOPGl sample was a single, uniformly thick (≈ 0.5 mm in thickness) sample. Sample orientations are known to an accuracy of better than 1° which was verified by the sample orientational dependence of $\Delta\mu x$ for the HOPGl sample. It is also assumed that the virgin HOPG and fibers have negligible mosaicity. (In the case of the fiber bundles this means that for an individual fiber the crystallite c axes are assumed to be strictly perpendicular to the fiber axis.) We have estimated the effect of mosaicity on our results, given reasonable estimates of mosaicity, and believe the effect to be quite small if not negligible.

The data which we present in this paper were obtained at the Stanford Synchrotron Radiation Laboratory using

the Si(220) monochromating Bragg reflection, but see Sec. V. The slit height of 1 mm was sufficiently small. Possibly the only experimental artifact in our results is the energy breadth of the white line and perhaps of other fine features of the near-edge spectrum related to the crystal monochromating conditions. We mention that results presented here are based on averaged intensities, averaged over from 3 to 10 individual experimental runs. However, individual runs were also examined for purposes of error estimates of integrals (over photon energy) of white-line spectra. Finally, as in previous work, only few orientations of $\hat{\epsilon}$ were considered. For the assumption of identical crystallite properties between HOPG and fibers, it is expected, due to the tensor component nature of the x-ray absorption and the known crystal structure of fibers, that the following orientations of $\hat{\epsilon}$ will yield identical results to one another: $\hat{\epsilon}$ perpendicular to the c axis in HOPG and parallel to the fiber axis in fibers; $\hat{\epsilon}$ at a 45° angle to the c axis in HOPG and perpendicular to the fiber axis in fibers. Results were obtained for the above orientations as well as for $\hat{\epsilon}$ at a 45° angle to the fiber axis in fibers.

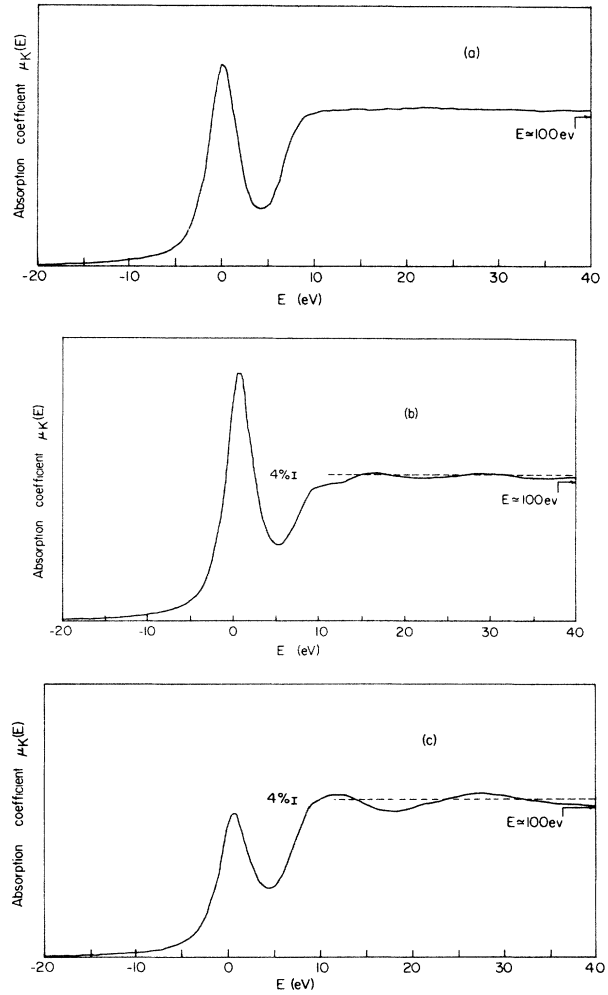

FIG. 1. Near-edge absorption spectra for (a) Br_2 vapor, (b) HOPGl in parallel orientation, and (c) HOPGl in rotated (45°) orientation. $E=0$ corresponds to a photon energy of 13 464.8 eV. Dashed lines correspond to the Br_2 vapor spectrum. The normalization was chosen at $E=100$ eV as indicated by the arrows and the size of the bars in (b) and (c) is $0.04\mu_K$ (100 eV). Actual scanning steps were 0.5 eV (2 eV) below (above) $E=8.5$ eV.

III. DETAILS OF ANALYSES

Since one of the main purposes of this work is to obtain an accurate and meaningful comparison of amplitudes for different sample orientations with respect to $\hat{\epsilon}$, it is appropriate to discuss the details of the analysis not ordinarily discussed in studies such as this.

The normalized quantity μ_K was obtained through extrapolation of the pre-edge μ by fits to both linear (in photon energy) and $\lambda^3-\lambda^4$ functions in the region 200 to 75 eV below the white line and through normalization to unity at a point ~ 90 eV above the main edge. The criteria for the normalization point were that it be at a particularly flat region of the spectra and as close as possible to the edge. In addition, for obtaining χ the energy dependence of the normalization factor was obtained through use of the McMaster fits. The post-edge background was obtained through least-square fits with the use of both cubic splines (fitted onto a $\lambda^3-\lambda^4$ function at high energy), and a piecewise continuous $\lambda^3-\lambda^4$ function. In fitting the background, several choices of degrees of freedom were also made. We estimate a less than 1% error in appropriate ratios of Br-Br EXAFS amplitudes and white-line areas arising from our normalization procedure (e.g., see Fig. 1) and perhaps a 4—7% error (depending on the particular sample, and for room temperature results) in Br-Br EXAFS amplitude scalar factor ratios arising from uncertainties in the background function. This latter estimate is based on results of our least-square and transform methods using various background functions. (We note that no Fourier filtering was done.) In our opinion, however, through direct data subtraction which was also done, it is possible to decrease the error caused by the background assumptions.

IV. Br_2 VAPOR EXAFS

In order to understand the EXAFS in Br graphite a knowledge of Br_2 vapor is of clear importance and it is for this purpose that we measure again the vapor spectrum and analyze it in some detail. We will make use of the vapor spectrum for extracting Br-C EXAFS as well as for comparisons of Br-Br EXAFS and white-line spectra. The quantity $\mu_K(E)$ and a fitted background curve are given in Fig. 2, where a linearly extrapolated pre-edge background was subtracted from the data to yield $\mu_K(E)$. The experimental and parametrized results for $k\chi(k)$ are shown in Fig. 3. Details of our parametrization are given below and in the Appendix. Note that χ is quite small and hence sensitive to the chosen background function at photon energies near the edge and also that the parametrized function shown as the dashed line in Fig. 3 is based on a somewhat improved background function at

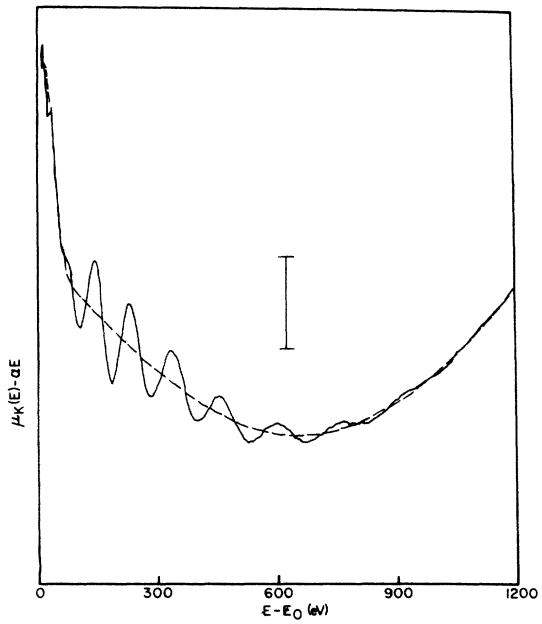

FIG. 2. Absorption spectrum of Br_2 vapor; $E_0=9.75$ eV. Dashed line represents a possible background function used to extract $\chi(k)$. The subtracted linear function αE was included for convenience of plotting. The vertical scale is given by the bar, whose size corresponds to $0.02\,\mu_K$ ($E=100$ eV).

lower energies than that shown in Fig. 2.

For $6<k<17$ Å^{-1} these data were analyzed by fitting to the Teo *et al.*[15]—Lee *et al.*[16] amplitude and phase function parametrizations, where the Teo *et al.* "experimental" parameters were used as well as $r=2.28$ and $\sigma=0.045$ Å. [We have made use of Eq. (1) with $N=1$, $\langle\cos^2\theta\rangle=\frac{1}{3}$ and $e^{-2r/l}=1$ to relate F to $k\chi(k)$]. In agreement with the data of Stern *et al.*[17] the amplitude

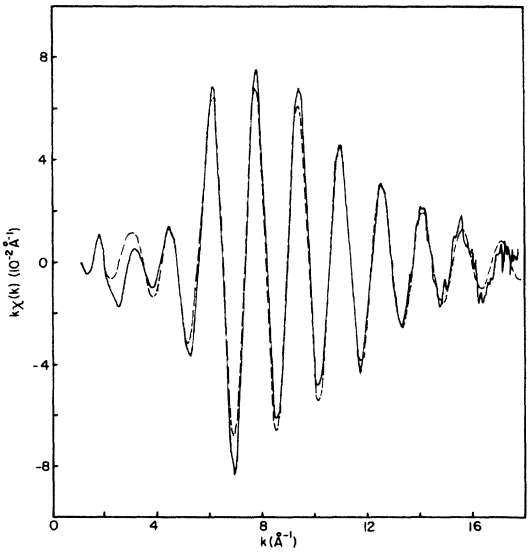

FIG. 3. EXAFS of Br_2 vapor. Solid line is based on results of Fig. 2 and on $E_0=9.75$ eV. Dashed line was fitted on the basis of Eq. (1) (also, see text).

scale factor A, treated as an adjustable parameter in our fits, was found to be larger than that corresponding to the data of Kincaid and Eisenberger[18] by about 30%. The value of E_0, also treated as an adjustable parameter, was found to be 9.75 eV (photon energy values, E, quoted in this paper correspond to differences with respect to the centers of the white lines). This value is in better agreement with the calculated value[18] of 12 eV than was Lee and Beni's[19] similarly extracted value of 7 eV.

Stern *et al.*,[17] who did not make use of theoretical fits, but rather used back Fourier transforms for determining the amplitude, concluded that the experimental amplitude was in agreement with Lee-Beni theory at $k=6$ Å^{-1} and that it fell below theory by $\sim 20\%$ at $k=8$ Å^{-1}. It can be seen that our results have verified these conclusions. On the other hand, the details of the approach of the experimental results to the Lee-Beni calculational ones as $k\rightarrow 6$ Å^{-1} from above is given somewhat differently by Stern *et al.* and by us. Our choices of background functions, used to extract $\chi(k)$, all yield an amplitude which is within $\sim 1\%$ of the Lee-Beni results at $k=7$ Å^{-1}, whereas Stern *et al.* find approximately a 10% discrepancy with theory at $k=7$ Å^{-1}. Thus we find a sharper transition to the Lee-Beni results than do Stern *et al.* The source of this difference is not clear. It could be either (a) a genuine experimental discrepancy; (b) a result of different choices of background functions; or (c) a result of the different methods of analysis used, since our result is based directly on the magnitude of the trough (see Fig. 3) in the experimentally determined $\chi(k)$ at $k=7$ Å^{-1}. Finally it is interesting to note that Stern *et al.* have interpreted the behavior of the amplitude in the region $k=6$–8 Å^{-1} in terms of multielectron effects.

The theoretical phase function in the standard EXAFS formula is seen to approximate our experimental results well since the parametrization is based on it down to $k=2.8$ Å. Nevertheless, there is a sharp decrease in the experimental *amplitude* from the theoretical one at low k. Rehr and Chou[20] have attributed a deviation of experiment from single-particle plane-wave-scattering theory at low k to spherical-wave corrections. They also found a spherical-wave effect in $\phi(k)$ and obtained agreement with experiment. However, upon choosing $E_0=9.75$ eV, as above, and suitably choosing the background at low k we obtained the above-mentioned agreement with the Lee and Beni theory for $\phi(k)$. It is stressed that our procedure for determining phases and amplitudes has been used chiefly as a working hypothesis for analyzing Br-graphite results and we do not suggest that spherical-wave effects are unimportant. In the remaining analysis of Br-graphite data we make use of this low-k parametrization only in the extraction of Br-C EXAFS. In particular, the amplitude of the Br-Br EXAFS contribution at low k is *scaled* on the basis of fits to the high k, essentially Br-Br, EXAFS.

V. CHECKS ON POLARIZATION

A crucial assumption made in our work on Br graphite is that of the linear polarization of the radiation field. While we attempted to position the sample where this

ought to be a valid assumption, i.e., where the incident synchrotron radiation is a maximum, and while we chose the slit to be small, it is useful to check this assumption further. Several types of checks can be made. One is to examine the effect of changing the Bragg reflection of the monochromating Si crystal. Another is to appropriately vary the orientation of the sample with respect to the beam. Another is to obtain results for different electron beam energies, and finally various sized slits can be chosen. In the course of these experiments all of these experimental configurations were used (although not for all samples or all polarization orientations) and *no* noticeable deviation from the expected linear polarization was observed. In particular, monochromating radiation from the (111) and (220) reflections was used and both parasitic and dedicated runs were made (giving different electron beam energies). Neither of these variations affected the EXAFS signal beyond about 10 eV past the main absorption edge. As expected, the breadth of the white line (WL) and sharp features within several eV of the main absorption edge (in parallel orientation only) are affected by differences in resolution between the (111) and (220) monochromating conditions. Also, using the (220), when slit heights were increased markedly from that used here (1 mm) a broadening in the WL and near-edge structure was observed as expected. Sample orientational checks were made on samples of HOPG and fibers. The HOPGv sample, originally oriented with the carbon planes perpendicular to the beam direction, was rotated 45° about an axis (y, see Fig. 4) parallel to the presumed electric-field polarization. The results for both the original and rotated orientations were identical to within the precision of the data. See Fig. 5 for the comparison of WL spectra. Other checks were made using the fibers. Parallel and perpendicular ($\beta=0°$ and $\beta=90°$ in Fig. 4) orientational transmission-mode measurements are necessarily taken with the fiber axes parallel to and perpendicular to the horizontal plane (plane of the electron beam), respectively. A check on the polarization was obtained by taking transmission-mode data for $\beta=45°$ but with the fiber axes in the horizontal plane (see Fig. 4). In this way we detect a possible component of the electric field along the vertical direction since its contribution would be the same for $\beta=0°$ and $\beta=45°$, but not for $\beta=90°$ in these orientations. This check is of importance, because when the incident x-ray beam is out of the central plane of the electron beam, then the absorbed radiation is elliptically polarized, i.e., there is a finite z component of the field. The result

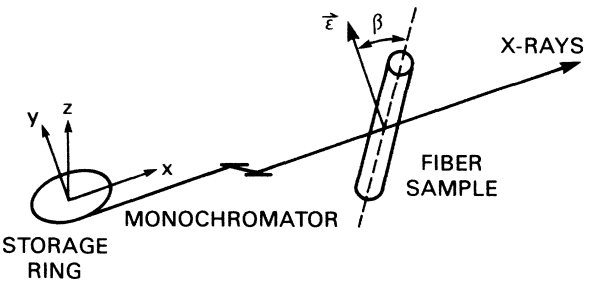

FIG. 4. Schematic of experimental configuration.

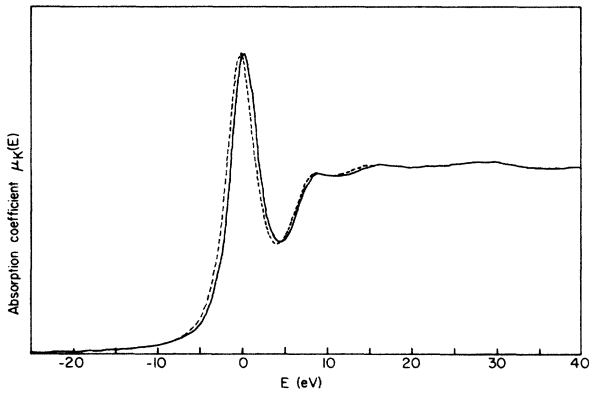

FIG. 5. Room temperature near-edge spectra of HOPGv in parallel orientation. Solid curve corresponds to the sample face, i.e., graphitic planes, being perpendicular to the x-ray beam and the dashed curve corresponds to the sample face being at a 45° slant to the x-ray beam.

was that the $\cos^2\beta$ dependence of μ [Eq. (2) of Ref. 1] was obeyed, that is, $\mu(E)$ for $\beta=45°$ was identical, to within the precision of the data, to the average of the $\beta=0°$ and $\beta=90°$ results. Furthermore, we obtained a satisfactory comparison between these data and fluorescence data (shown in Ref. 1) taken in a separate experiment for $\beta=90°$ and $\beta=45°$, and for the same samples and sample orientations with respect to the beam as for the transmission data.

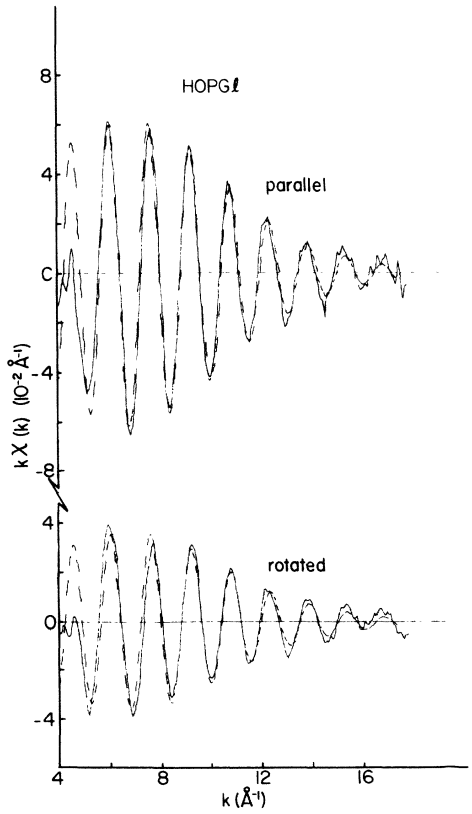

FIG. 6. EXAFS of HOPGl. Comparison of Teo *et al.* fits (dashed curves) with experiment; $E_0=3$ eV. Structural parameters used in the fits are $r=2.31$ Å and $\sigma=0.06$ Å.

VI. Br-Br EXAFS RESULTS FOR GIC-Br

Our experimental results for $k\chi(k)$ are presented in Figs. 6–9. Least-square fits of the Teo *et al.*—Lee *et al.* parametrizations to the experimental $\chi(k)$ were made, and they are seen to be accurate (Figs. 6–9). The resulting value of the room temperature Debye-Waller exponent appears to be slightly greater in magnitude for the Br-graphite systems than for Br_2 vapor. Perhaps this is consistent with the down-shift in intercalate Raman frequency[11] from the Br_2 vapor result. The value of σ which gives agreement with our data on GIC-Br materials at $T=300$ K is 0.06 Å, as compared to the corresponding value 0.045 Å for Br_2 vapor. (However, a direct comparison, not shown here, of the k dependences of Br-Br EXAFS peak heights between Br_2 vapor and HOPGl suggests that the difference in σ values between the two materials is only ~ 0.005–0.01 Å.) As also previously reported,[2] we find $r=2.31$ Å and E_0 to lie 3 eV above the center of the white line. These values are consistent with all of the Br-graphite data. For purposes of comparison the amplitude scale factor A used here is defined in terms of $\chi(k)$ precisely as it was in the case of our analysis of data for Br_2 vapor except for the fact that σ and r [only in the denominator of Eq. (1)] are of course allowed to vary from the case of Br_2 vapor. Values of A were thereby obtained through least-square fits, keeping E_0, r, and σ fixed at the above-mentioned values. All other electronic parameters given by Teo *et al.*—Lee *et al.* were also kept fixed at the Teo *et al.* (expt.)—Lee *et al.* values. The results for A are given in Table I. Also included in the table are peak heights of the magnitudes of the Fourier transforms (MFT) of $k^n\chi$ with $n=1$ and $n=3$. The

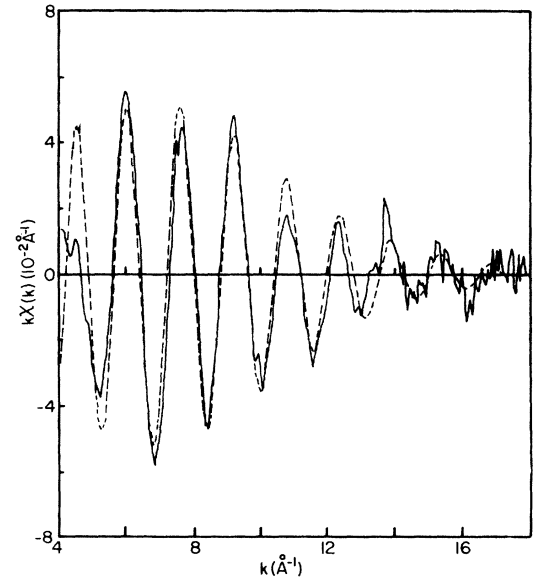

FIG. 8. EXAFS of sample HOPGv at $T=400$ K in parallel orientation. Same comparison is made as in Fig. 6.

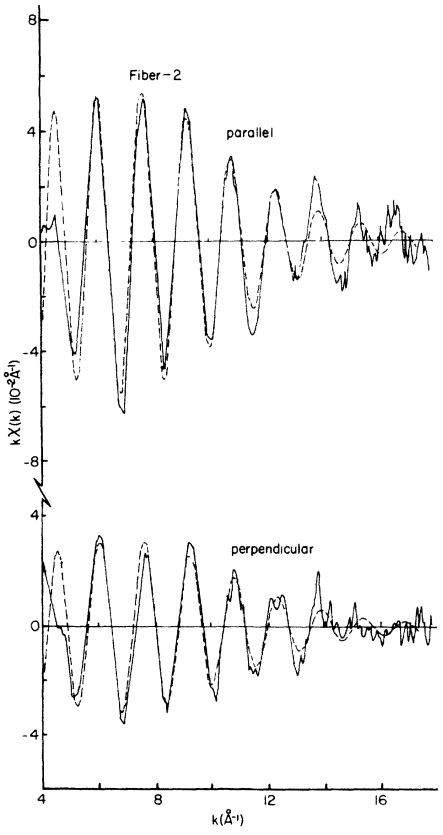

FIG. 7. EXAFS of sample fiber-2. Same comparison is made as in Fig. 6.

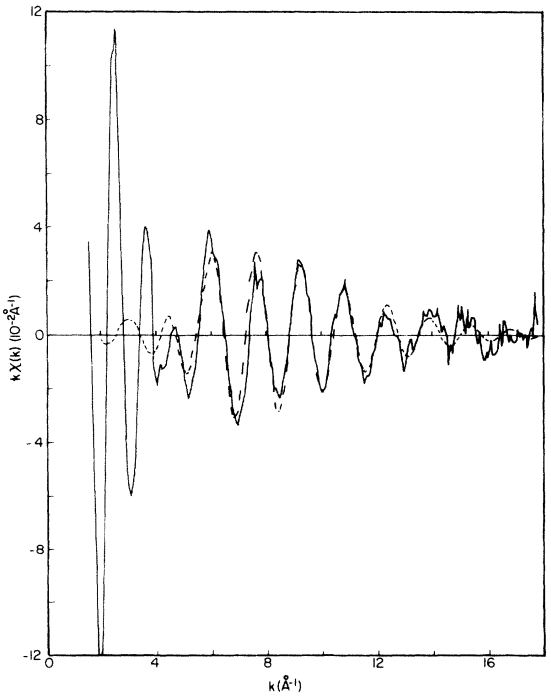

FIG. 9. EXAFS of HOPGv at room temperature in rotated (45°) orientation. Comparison of "improved" Teo *et al.* fit with experiment. Same E_0 and parameters as in Fig. 6.

TABLE I. Br-Br EXAFS amplitude properties. Parallel and rotated are denoted by par. and rot., respectively. (Fourier transform magnitudes and fitted amplitudes correspond to the range $4.7 \leq k \leq 17.7$ Å^{-1}.)

Quantity		Least-square-fit[a] amplitude, A (units of Å)		Peak height in Fourier transform magnitude k weighting (arb. units)		Peak height in Fourier transform magnitude k^3 weighting (arb. units)	
Orientation		par.	rot.[b]	par.	rot.[b]	par.	rot.[b]
Fiber-1 (300 K)		0.470 (68)	0.260 (104)	0.470	0.267	0.470	0.278
Fiber-2		0.447 (63)	0.259 (47)	0.439	0.258	0.429	0.235
HOPGv	300 K	0.414 (48)	0.240 (68)	0.408	0.234	0.399	0.218
	360 K	0.418 (63)	0.234 (78)	0.397	0.207	0.383	0.190
	400 K	0.423 (85)	0.236 (88)	0.393	0.208	0.372	0.181
HOPGl		0.503 (44)	0.297 (49)	0.496	0.304	0.492	0.299

[a]Based on fit of $\chi(k)$ to Teo *et al.*—Lee *et al.* parametrized theory with $E_0 = 3$ eV, $r = 2.31$ Å, and $\sigma = 0.06$ Å. Values in parentheses are proportional to variances of least-square fits.
[b]Values for fibers and HOPG correspond, respectively, to 90° and 45° rotation (see text).

peak height of the $n = 3$ Fourier transform of high-temperature results and all fiber-1 results are probably most uncertain of all of our results because of poor data in the large-k region, so these values must be discounted in our determination of the angle α. Examples of MFT's are given in Fig. 10. (No structure other than nearest-neighbor distances are seen.) Through a comparison of the positions of the maxima of MFT's we have also determined that for a common value of E_{0_c} of 9.8 eV the nearest-neighbor Br distance is ~ 0.06 Å greater in Br graphite than in Br_2 vapor instead of the 0.03 ± 0.01 Å difference which was based on our least-square fits to the Lee *et al.* phase parametrization. We obtain values of the angle α from appropriate ratios of the EXAFS quantities in Table I. For example, in the case of all room temperature data, ratios are seen (Table II) to be between 0.55 and 0.61 which, through use of Eqs. (1) and (2) of Ref. 1, correspond to $\alpha = 12.5°$ and $\alpha = 18.5°$, respectively. Different orientational data are directly compared in Fig. 11. From this figure it can be seen that a lower limit of the 45°-rotated-to-parallel-amplitude ratio is 0.55 (0.57) for HOPGv (HOPGl) and that there is a weak k dependence of this ratio; in the region $7 \leq k \leq 9$ Å^{-1} the ratio appears to be smaller than in neighboring regions. The small displacement in k between the peak maxima of different orientational data of both Figs. 11(a) and 11(b) at $k \approx 6$ Å^{-1} is possible due to the presence of Br-C EXAFS; in Fig. 11(b) there also exists a slight E_0 effect (see figure caption). With regard to the temperature dependence of the ratio, there is no suggestion of an increase with in-

TABLE II. Anisotropy of Br-Br EXAFS.

Material	Temp. (K)	Least-square-fit amplitude, A[a]	Peak height in Fourier transform magnitude[a] k weighting	k^3 weighting
Fiber-1	300	0.552	0.570	0.592
Fiber-2	300	0.580	0.588	0.548
HOPGv	300	0.581	0.574	0.547
	360	0.560	0.522	0.497
	400	0.558	0.530	0.487
HOPGl	300	0.590	0.612	0.609

[a]Values are ratios of rotated to parallel orientational results of Table I.

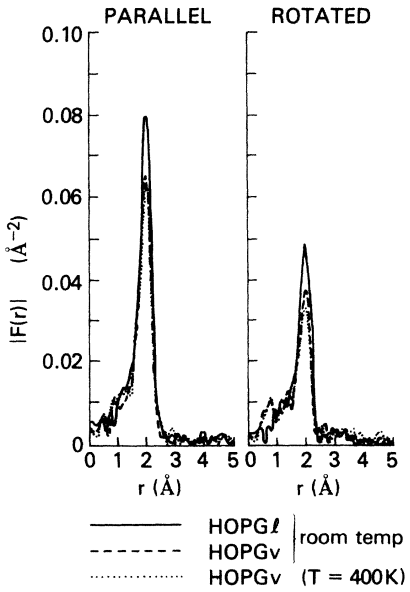

FIG. 10. Magnitude of Fourier transform of $k\chi(k)$. Region of integration is 4.7 Å$^{-1} \leq k \leq 17.7$ Å^{-1}.

creasing temperature. Such a result would be expected if the nonzero angle α were an out-of-plane thermal-vibrational effect. Also there is no substantial decrease in EXAFS signal upon increasing T beyond the "melting" temperature, as seen in Table I and by comparing Figs. 8 and 11(b). Thus, we conclude that Br-sublattice melting does not appreciably affect nearest-neighbor Br-Br bonds, since melting can reasonably be presumed to have occurred in our HOPG-based sample.

The comparison of the spherical average of the amplitude scale factors with the amplitude scale factor for Br_2 vapor is now considered (Table III). If, for example, all of the bromine in the material were paired in strong Br_2-like molecular bonds these two quantities would be expected to be the same on the basis of the assumption of "amplitude transferability." Clearly that is not found to be the case as the averaged values are substantially the lesser of the two. There also exists a large discrepancy in amplitudes of Br-Br EXAFS between the two HOPG samples. We await discussion of our white-line and Br-C EXAFS results of Secs. VII and VIII to discuss these Br-Br EXAFS results further. Similar amplitude discrepancies between Br_2 vapor and Br adsorbed Grafoil were noted by Heald and Stern.[4] However, Heald and Stern may have obtained too small a discrepancy, because their Br_2 vapor EXAFS amplitude was in agreement with that of Kincaid and Eisenberger,[18] shown to be too small by $\sim 30\%$ by the later improved experiments of Stern *et al.*[12] as we stated earlier.

In the case of HOPGl, data are sufficiently precise for utilizing data subtraction to study the anisotropy of Br-Br EXAFS. We computed the quantity $\delta\mu \equiv K\mu_{0^\circ} - \mu_{45^\circ}$ for various constant values of K. Depending on the value of K, the Br-Br oscillations were found to be absent in $\delta\mu$ over *limited* regions in K. Defining $K_R(k)$ to be the appropriate ratio of Br-Br EXAFS amplitudes, we find

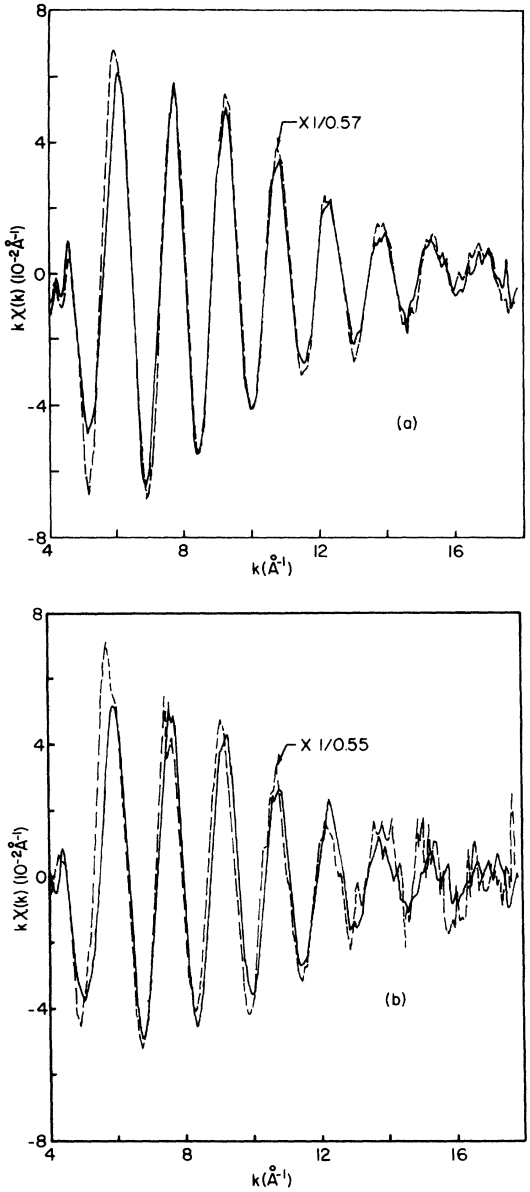

FIG. 11. Comparisons between different orientations in room temperature Br-Br EXAFS. Rotated orientational results for $k\chi(k)$ were multiplied by the values shown in the figure to obtain the dashed curves. Solid curves correspond to parallel orientational data. Data for HOPGl (a) and HOPGv (b) are based on $E_0 = 3$ eV, except the dashed curve in (b) for which $E_0 = 0$ for clarity.

$K_R(k) = 0.57$–0.58 in the region $8 \leq k < 10$ Å^{-1} and $K_R(k) = 0.63$–0.64 in the region $10 < k \leq 14$ Å^{-1}. However, this variation in K_R is probably within our experimental uncertainty and the latter region results are clearly most uncertain of all due to the smallness of χ in that region.

Finally, we observe no difference between fibers and HOPG with regard to the orientation of Br nearest-neighbor pairs. Nevertheless, it is possible that the bromine within the fibers is not truly intercalated, but rather adsorbed onto the individual crystallites.

TABLE III. Spherical averages of Br-Br EXAFS amplitudes. Results are based on those of Table I (aside from units); the spherical average of A is given by $\frac{1}{3}(2A_{\text{rot}}+A_{\text{par}})$, etc.

Material	Temp. (K)	Least-square-fit amplitude, A (units of Å)	Peak height in Fourier transform magnitude, k weighting (arb. units)	Peak height in Fourier transform magnitude, k^3 weighting (arb. units)
Fiber-1	300	0.330	0.330	0.330
Fiber-2	300	0.322	0.314	0.289
HOPGv	300	0.298	0.287	0.269
	360	0.295	0.266	0.245
	400	0.298	0.266	0.236
HOPGl	300	0.366	0.363	0.350
Br_2 vapor	300	0.487[a]		

[a]Based on fit of $\chi(k)$ to Teo *et al.*—Lee *et al.* parametrized theory with $E_0=9.75$ eV, $r=2.28$ Å, and $\sigma=0.045$ Å.

VII. WHITE LINES

White-line (WL) spectra are to some degree, sensitive to the chemical environment of the absorbing atom. For example, substantially different near-edge features are seen in $S_4N_3Br_3$, bromobenzene (Ref. 13) (C_6H_5Br) and bromine-doped polyacetylene (Ref. 13) than in Br_2 vapor. On the other hand, for both KBr (Ref. 21), an ionic material with a filled $4p$ shell, and $(SNBr_{0.4})_x$ (Ref. 12), for which Br-Br EXAFS results[12] indicated the predominance of either Br_3^- or other polybromide ions, strong WL features were observed at precisely the photon energy corresponding to the WL of Br_2 molecules. The theory of WL's is of current interest but no calculations, to our knowledge, have yet been done for Br_2. Generally, dipole first-order perturbation transitions or multiscattering effects, i.e., shape resonances,[22] have been proposed for explaining WL spectra. Heald and Stern,[4] assuming a $1s$ to $4p\sigma^*$ dipole first-order perturbation transition to be the origin of the WL in Br_2, noted that the anisotropy of the WL intensity is expected to be the same as that of Br-Br EXAFS (Ref. 23), i.e., to be given by $\langle\cos^2\theta\rangle$. Indeed, their results on Br_2 adsorbed Grafoil were that the Br-Br EXAFS amplitudes and WL energy integrals displayed a common anisotropy. On the other hand, they found too small a spherically averaged WL intensity in comparison to that of Br_2 vapor.

Comparisons of some of our WL spectra are given in Fig. 12. In the case of our thin samples the WL spectra for different orientations scale with respect to one another by factors consistent with our Br-Br EXAFS—seen by noting the results for WL spectra in Fig. 12 and the EXAFS results of previous figures and tables. Only results for the (thick) HOPGl sample deviate slightly from scaling behavior, and perhaps this is indeed a thickness effect.[24] The generally observed scaling feature of our WL spectra suggests that the main-edge contribution is negli-

TABLE IV. Area under white line. Arbitrary units. Integrations are from $E=-20$ to $E=0$ eV, the position of the maximum absorption.

Orientation →		Par.	Rot.[a]
Fiber-1	300 K	0.470	0.293
	360 K	0.466	0.284
	400 K	0.467	0.290
Fiber-2		0.440	0.294
HOPGv	300 K	0.429	0.279
	360 K	0.437	0.269
	400 K	0.428	0.272
HOPGl		0.438	0.267

[a]See footnote (b) of Table I.

TABLE V. Anisotropy and spherical average of area under white line.

Material	Temp. (K)	Anisotropy[a]	Spherical average[b] (arb. units)
Fiber-1	300	0.624	0.330
	360	0.610	0.322
	400	0.622	0.327
Fiber-2	300	0.668	0.320
HOPGv	300	0.651	0.307
	360	0.616	0.304
	400	0.635	0.304
HOPGl	300	0.610	0.304
Br_2 vapor	300		0.317

[a]Ratios of rotated to parallel orientational results of Table IV.
[b]Based on results of Table IV.

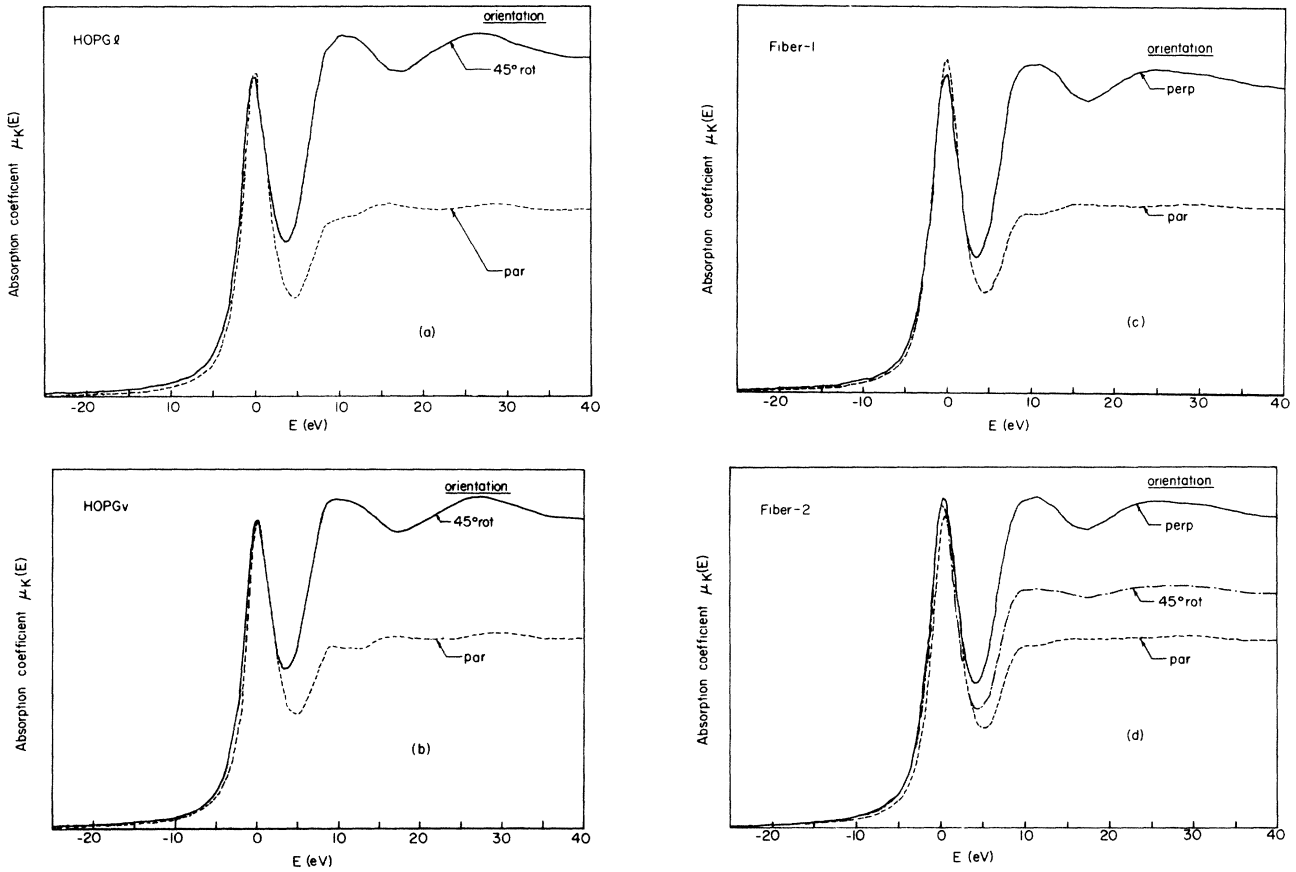

FIG. 12. Comparisons between different orientations in room temperature white-line spectra. For HOPG*l* (a) and HOPG*v* (b) scale factors of 1/0.55 and 1/0.60 are used, respectively, to obtain agreement in the peak heights of the rotated (45°) and parallel orientational data. For fiber-1 (c) the results of a scale factor of 1/0.6 is shown in comparing perpendicular and parallel orientational data and for fiber-2 (d) scale factors of 1/0.8 and 1/0.6 are used, respectively, to compare 45°-rotated and perpendicular orientational data with parallel orientational data. Peaks were adjusted horizontally for visual alignment.

gible over most of the WL spectrum in our experiments. Energy integrals (for energies up to peak maxima) of WL spectra were also computed through a linear interpolation of the data. Results are given in Tables IV and V.

Additionally, following Heald and Stern's technique for obtaining an estimate of the main-edge contribution in the WL region, we considered the quantity $\mu_\perp$ which we define as the absorption coefficient corresponding to perpendicular orientation in the case of intercalated HOPG. For our materials, however, it is necessary to make use of the cylindrical symmetry relation, $\mu_\perp = 2\mu_{45°} - \mu_{||}$. Reasonable results (see Fig. 13) seem to have been obtained for our HOPG*v* sample, although such results are particularly sensitive to variations in energy resolution among experimental runs and may be somewhat inaccurate. The estimated background contribution shown by the dotted line in Fig. 13 would lead to a 5–7% decrease in the ratio of rotated to parallel orientational WL areas from the values obtained with no background correction. However, we regard this solely as an upper limit to the background correction at least for HOPG*v* data. Most likely the main edge contributes negligibly below the peak maxima for reasons based on the observed spectral shapes.

Comparisons between Br_2 vapor and Br-graphite WL intensities are also of interest. The essential agreement between the two is apparent, as seen in Table V (also, Fig. 1 of Ref. 2) where spherically averaged results are compared with those of Br_2 vapor. Areas (i.e., energy integrals) agree to better than 4%. Thus, at least within the first-order transitional interpretation and to within this 4% ac-

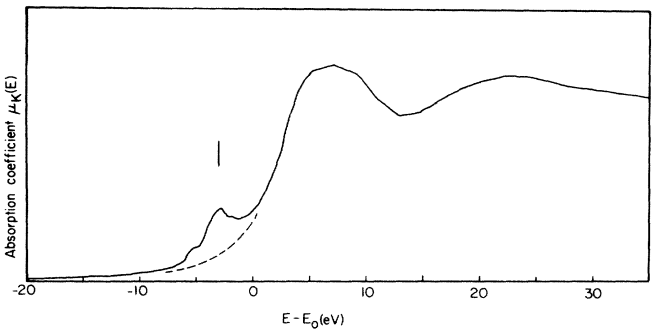

FIG. 13. Near-edge absorption spectrum, in perpendicular orientation, for HOPG*v* at room temperature. Results are for $\mu_\perp$, defined as $2\mu_{45°}-\mu_{||}$. Dashed line is a "hand-drawn" extrapolation of the main edge. Position of vertical line corresponds to a photon energy of 13 465 eV.

curacy our data show no indication of charge transfer to $4p$ states or distortion of such states from the case of Br_2 molecules.

In addition, our WL results are seen to depend little on sample (where we compare HOPG-45° with fiber-$\perp$, etc.) or temperature. In view of the above-mentioned possible sensitivity of WL spectra to chemical bonding the quantitative agreement of the WL spectra among all of our Br-graphite samples as well as that between our spherically averaged spectra and the spectrum of Br_2 vapor is quite striking. These results are apparently consistent with the possibility that the bromine is in the form of essentially Br_2 molecules. In that case the peculiarities seen in the EXAFS spectra must be explained in terms of electronic effects related to the environment of the Br_2 molecules. In particular, perhaps graphite-plasmon excitations[25] give rise to the decreased amplitudes. Unfortunately, it is not known whether or not these results are also consistent with the existence of polybromide ions, as the latter have been concluded to be predominant on the basis of a recent interpretation[26] of x-ray diffraction data on desorbed samples. Nevertheless, in this regard, our EXAFS results give no indication of a second neighbors Br-Br peak in the Fourier transforms at about twice the nearest-neighbor distance. That result would suggest the existence of polybromide ions and has been observed in other[12,13] bromine compounds, but not GIC-Br.

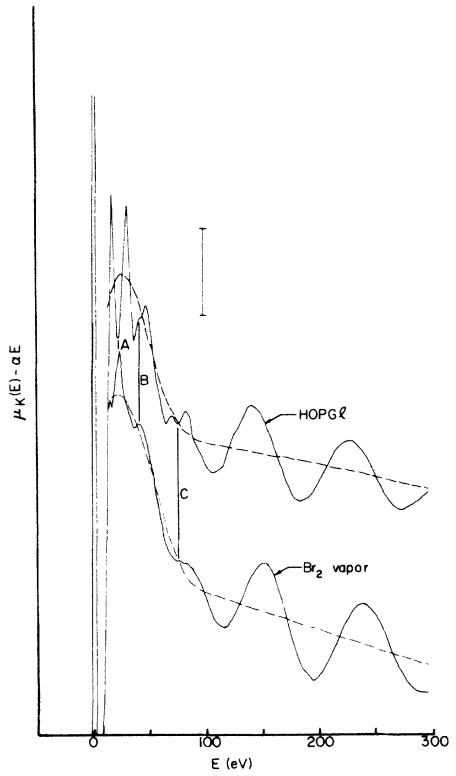

FIG. 14. Room-temperature absorption spectra of Br_2 vapor and HOPGl (in parallel orientation). The bar represents 0.02 μ_K ($E=100$ eV) and the linear subtracted-out functions αE were chosen to cross the corresponding $\mu_K(E)$ at the upper energy limit of the data, i.e., $E=1200$ eV, and at $E=100$ eV. Dashed curves are fitted background functions.

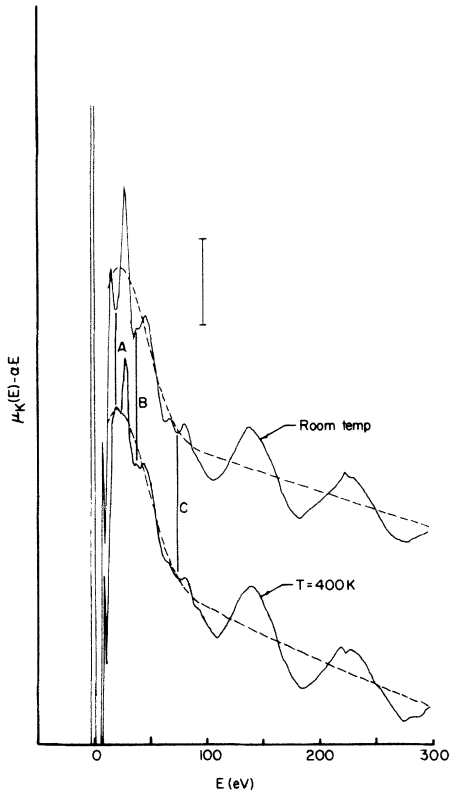

FIG. 15. Absorption spectra of HOPGv (in parallel orientation) at room temperature and at 400 K. See also figure caption to Fig. 14 and text.

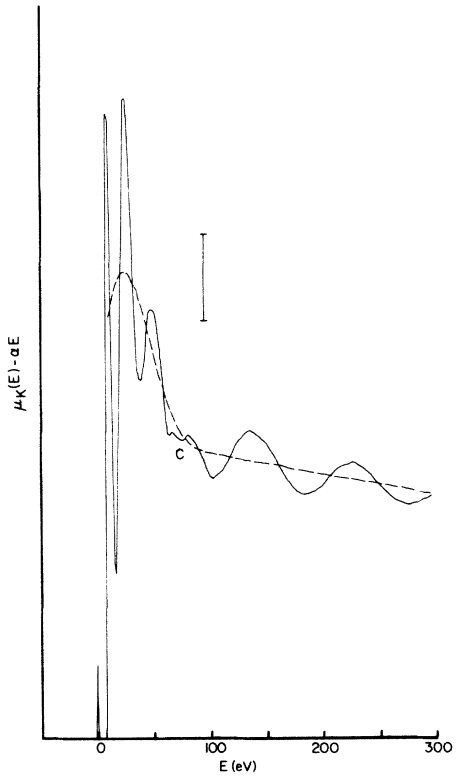

FIG. 16. Absorption spectrum of HOPGl (in 45°-rotated orientation). See also figure caption to Fig. 14 and text.

VIII. Br-C EXAFS AND *NON*-NEAREST-NEIGHBOR Br-Br EXAFS

In order to extract the Br-C EXAFS contributions to the data we need to understand the Br-Br EXAFS contribution (this is especially true for parallel orientation). That it is possible to reasonably assume a nearest-neighbor Br-Br EXAFS contribution similar to that for Br_2 vapor is indicated in Figs. 14 and 15. In those figures correspondences are seen between features in the spectra for Br_2 vapor and GIC-Br (parallel orientation) from high energies down to the edge. These correspondences are marked in Fig. 14 by the straight lines between vapor data and HOPG*l* data and appear to be in accord with a *common* E_0 value. Whereas the lowest energy feature indicated in the vapor data, denoted A, is not apparent in the data for HOPG*v* or HOPG*l* at room temperature, it is indeed apparent in the data (Fig. 15) for HOPG*v* at $T=400$ K. Presumably the reason for this is that Br-C EXAFS and distant-neighbor Br-Br EXAFS have sufficiently decreased in magnitude at $T=400$ K that the corresponding nearest-neighbor peak, which can be expected to be only weakly temperature dependent, has become observable. That the nearest-neighbor contribution is weakly temperature dependent is both physically reasonable and directly observable in the high-k region of the data. Furthermore, the structure in the GIC-Br data additional

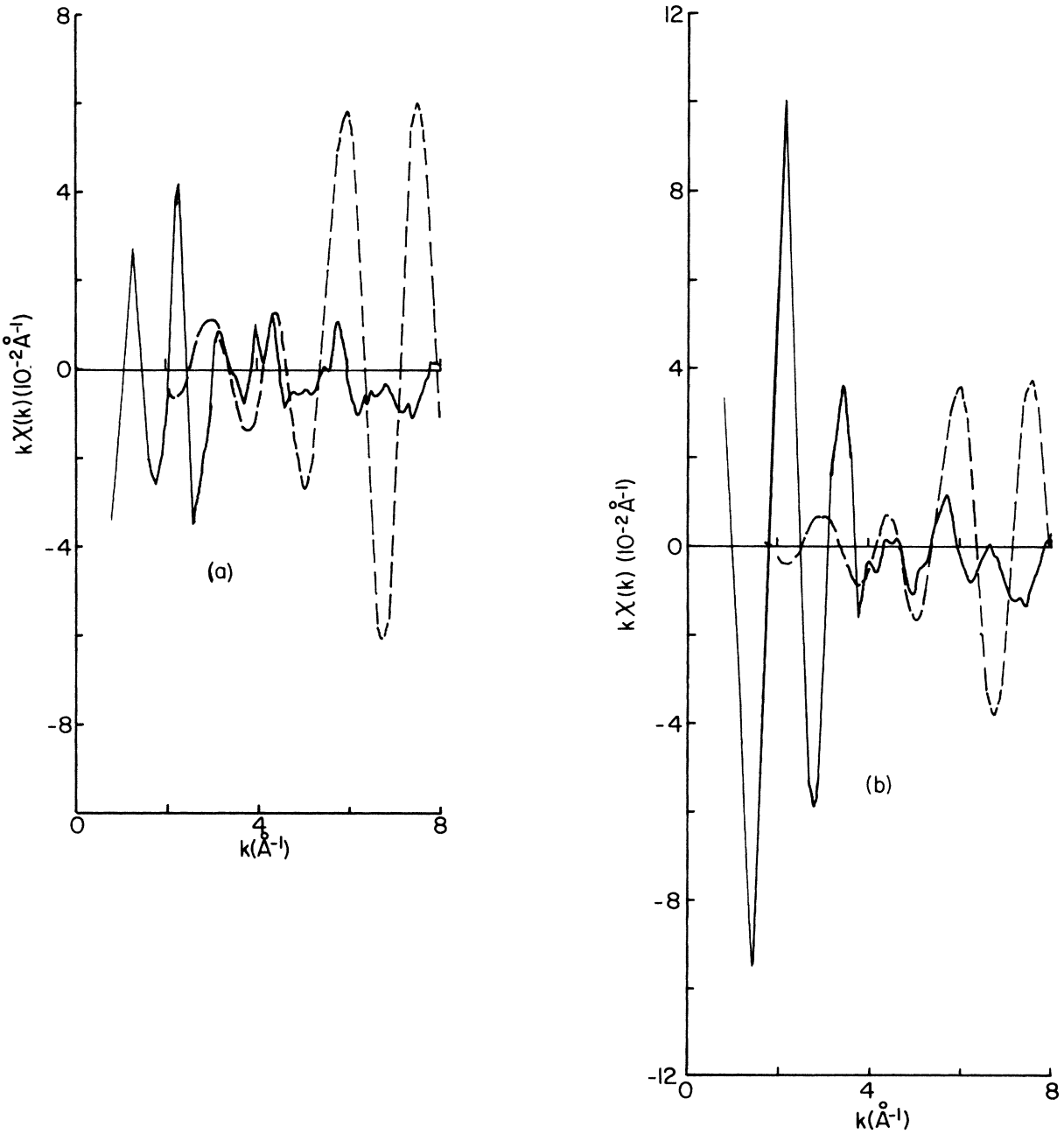

FIG. 17. Extracted Br-C EXAFS for HOPG*l*. Results are based on $E_0=9.75$ eV. Dashed lines represent subtracted-out nearest-neighbor Br-Br EXAFS (see text). Parallel orientational results are shown in (a) and 45°-rotated orientational results are shown in (b).

to that in the Br_2 vapor data in the region of C (see Fig. 14) appears to correspond to distant-neighbor Br-Br EXAFS by virtue of the fact that it occurs at identical energies in both orientations and that it appears to be about twice as large in parallel orientation as in 45° orientation (compare Figs. 14 and 16). This is precisely what one would expect for Br pairs lying parallel to the graphite planes. (Figures 14 through 16 also provide an illustration of the accuracy of our normalization procedure. All data were normalized at the energy corresponding to the vertical bar, whose length also gives the vertical scale. Since χ is seen to be less than 0.005 in that region of energies the only possible non-negligible normalization-derived uncertainty is the pre-edge extrapolation which is estimated to be $\sim 1\%$.)

Thus, it makes sense to attempt to subtract from the data the nearest-neighbor Br-Br contribution in the spirit of an EXAFS picture even at low k. We do this for $k \geq 2$ Å^{-1} using our parametrization of the Br_2 vapor data. Results are shown for HOPGl in Fig. 17. In that figure $E_0 = 9.75$ eV was used, and the theoretical amplitude was scaled to fit the high-k results for GIC-Br in each orientation; the structural parameters used in the theoretical (subtracted-out) expression were $r = 2.34$ and $\sigma = 0.06$ Å, and a non-Gaussian term in the phase of $-0.064\ k^3$ was also included (see a following section). In addition, in Fig. 18 we show similarly extracted EXAFS of HOPGl and HOPGv (at room temperature) based on $E_0 = 3$ eV and on structural parameters in the theoretical expression of $r = 2.31$ and $\sigma = 0.06$ Å. It is evident from the plots in Figs. 17 and 18 that the extracted EXAFS corresponding to parallel orientation is quite sensitive to the assumptions used in performing the extraction especially for $k \geq 3$ Å^{-1}. Also evident in Fig. 18 is the near identity of the extracted EXAFS of HOPGl and HOPGv.

The overall comparison (Figs. 19 and 20) of results for $k\chi(k)$ among different temperatures and materials is also informative. It is noteworthy that the observed temperature dependence of the EXAFS at low k, i.e., mainly Br-C EXAFS,[4] is much stronger than that of the high-k, nearest-neighbor Br-Br EXAFS, since at low k, Debye-Waller effects are generally minimal. In the case of the fibers the temperature dependence of the Br-C EXAFS signal, which is much less than in the case of HOPGv, may indeed simply be a Debye-Waller effect; the corresponding room temperature value of σ for the Br-C atomic pair is found to be about 0.15 Å. Furthermore, the large difference in Br-C EXAFS temperature dependence between fibers and HOPGv could possibly be indicative of the lack of a Br sublattice in the fibers down to 300 K. We assume that a Br melting transition took place in our HOPGv sample as expected from x-ray diffraction results on Br-HOPG. Consistent with this explanation of differences between fiber and HOPGv results we find that at $T = 400$ K, i.e., above the expected melting temperature in Br-HOPG, HOPGv and fiber-1 samples have nearly identical EXAFS properties. Finally, the identity in Br-C EXAFS between HOPG and fiber samples at $T = 400$ K also provides some indication that the fibers are intercalated rather than adsorbed.

Since it can be reasonably presumed that the HOPG-

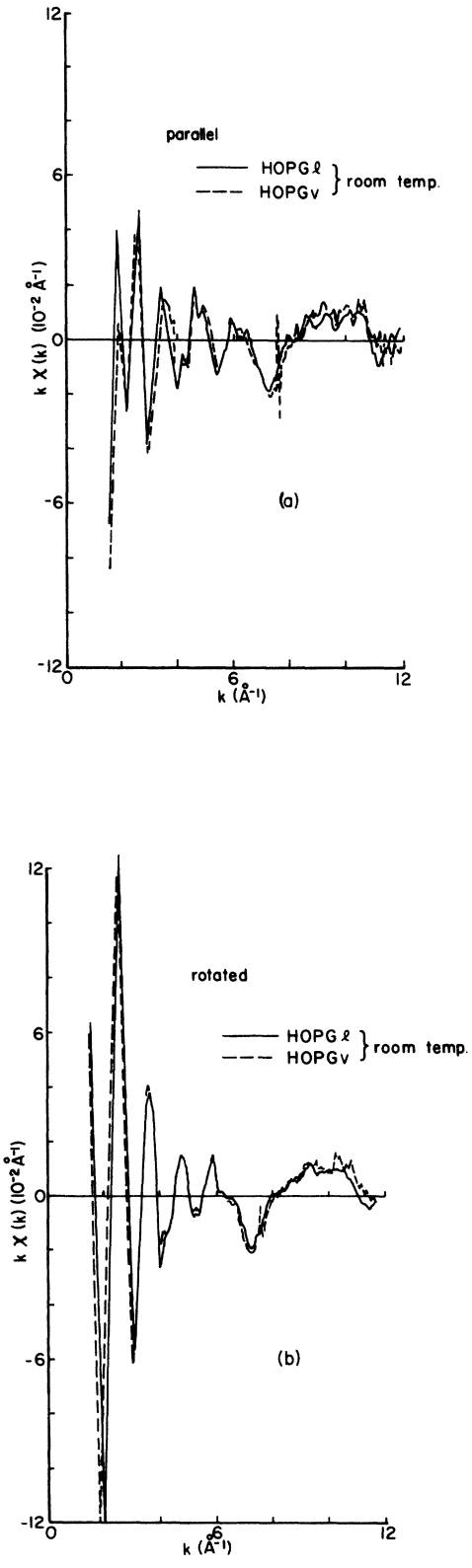

FIG. 18. Extracted Br-C EXAFS for HOPGl and HOPGv at room temperature. Results are based on $E_0 = 3$ eV. Parallel orientational results are shown in (a) and 45°-rotated orientational results are shown in (b). Subtracted-out nearest-neighbor Br-Br EXAFS on which these results are based is discussed in text.

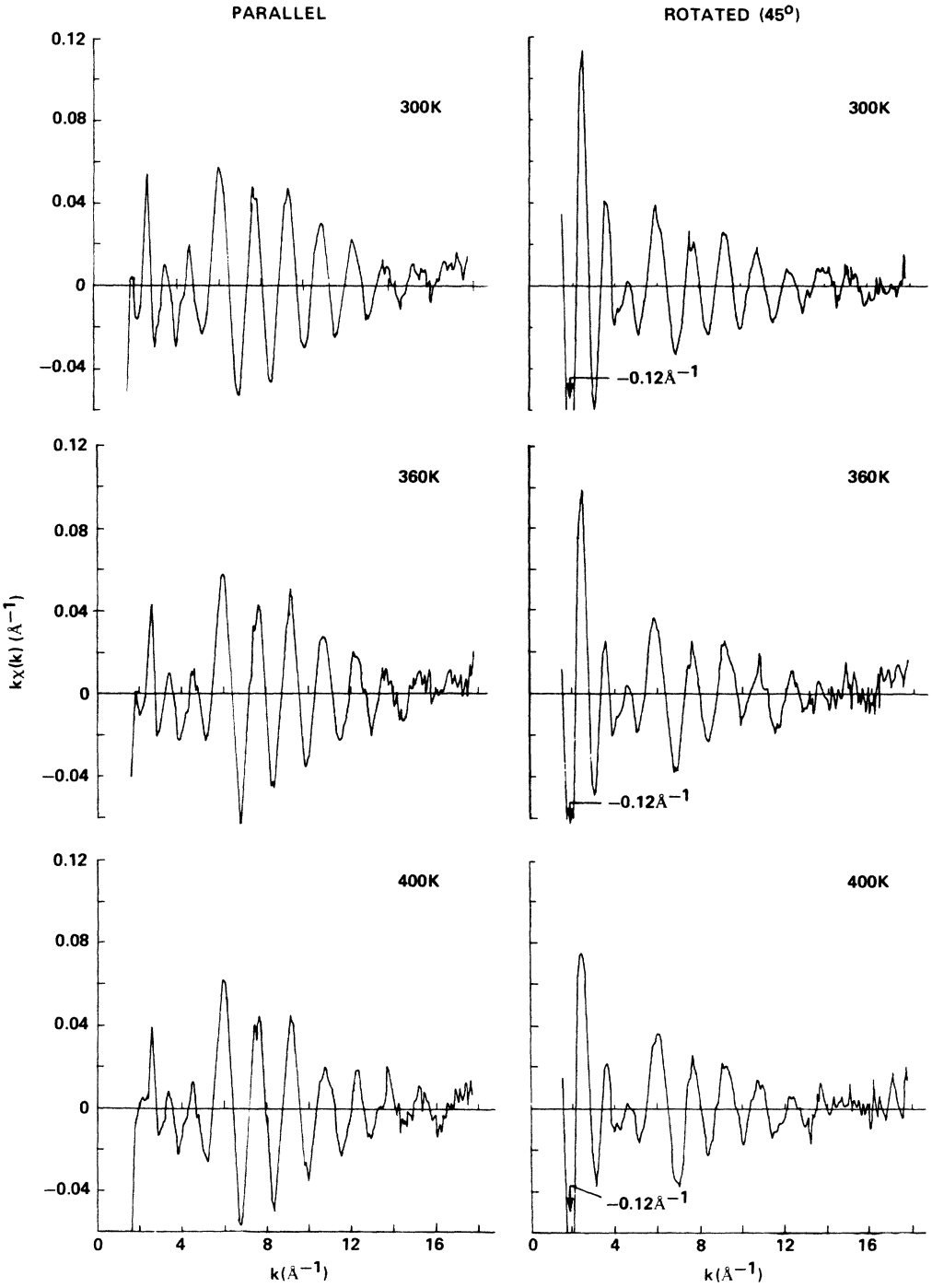

FIG. 19. $k\chi(k)$ for HOPGv as a function of temperature and orientation. Results are based on $E_0 = 3$ eV.

based sample HOPGv did indeed undergo the Br-sublattice commensurate-incommensurate and melting transitions, it is worth considering our EXAFS results for that sample further. That the absence of a qualitative change in shape of Br-C EXAFS upon melting may be in accord with particular models of ours will be shown in the following section. Also, the absence of evidence in our high-k data of more distant Br-Br neighbors than nearest neighbors does not necessarily imply randomly situated Br_2 "molecules." For example, using the Eeles and Turnbull[27] structural model for obtaining further-neighbor distances and coordination numbers, we have found that a reasonably increased value (from that of nearest-neighbor EXAFS) of σ can lead to a negligibly small EXAFS contribution from second-neighbor interatomic separations, even for k as low as 5 Å^{-1}.

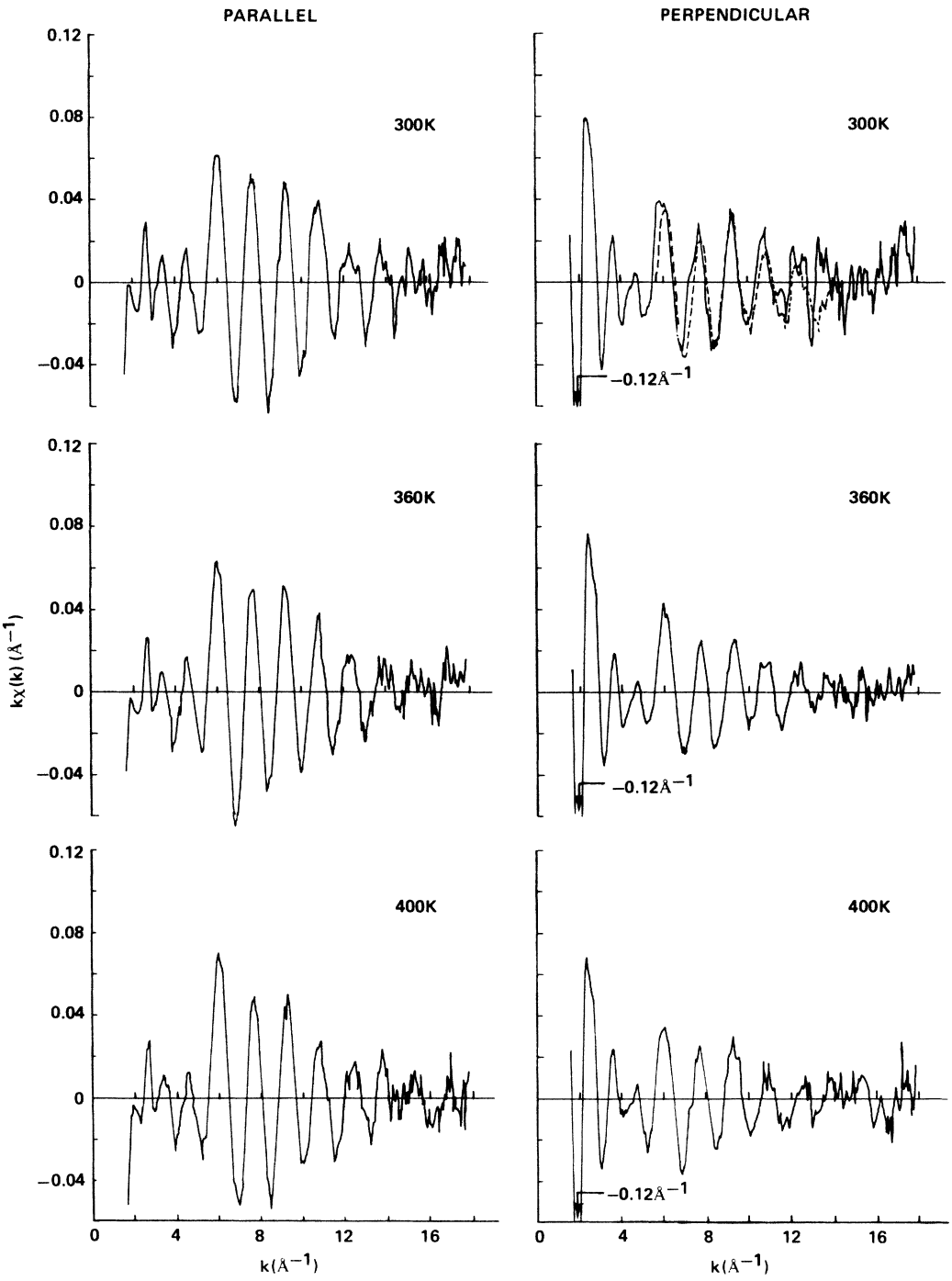

FIG. 20. $k\chi(k)$ for fiber-1 as a function of temperature and orientation. The solid curves are based on $E_0=3$ eV. The dashed curve corresponds to $E_0=0$ eV and to measurements in synchrotron conditions ("dedicated" mode of operation) different from those corresponding to the solid curves ("parasitic" mode of operation).

IX. MODEL CALCULATIONS OF Br-C EXAFS

We have performed model calculations of Br-C EXAFS in the single-atom and plane-wave-scattering approximation. These are based on computed[28] phase and amplitude functions and on several structural models. For structural models we make use of in-plane bromine sublattice models of Ghosh and Chung[26] (GC) and of Eeles and Turnbull[27] (ET) as well as a model corresponding to a two-dimensionally uniform distribution of Br atoms. The former two models have a basis in x-ray diffractional results for Br-superlattice reflections. The Br positions with

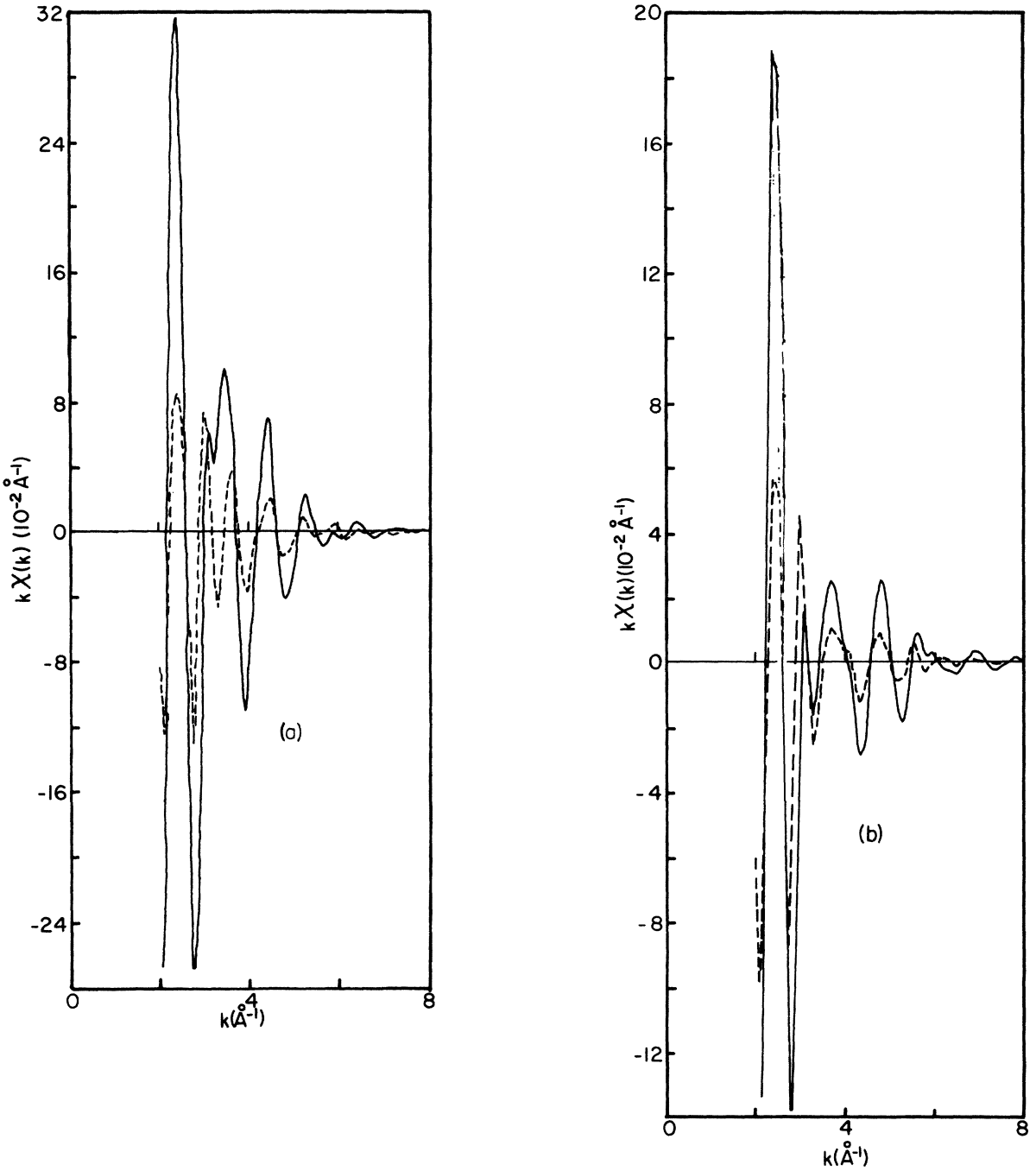

FIG. 21. Model calculation of Br-C EXAFS. For the case of intercalated HOPG the solid (dashed) line corresponds to 45°-rotated (parallel) orientational results. The structural models employed were (a) a Ghosh-Chung (Ref. 26) in-plane model; (b) a Ghosh-Chung model with out-of-plane components; (c) an Eeles-Turnbull (Ref. 27) model with out-of-plane components; and (d) a two-dimensionally uniform distribution model (see text). The same values of electronic parameters and of σ were used for all results (see text).

respect to the C positions were only determined in terms of a two-dimensional projection.[26] In all models we also make use of the following well-established[6,9,27,29] structural properties: A-A stacking of C planes which bound intercalate layers, a c-axis distance of 7.0 Å between those C planes, and a 3.35 Å c-axis distance between other (A-B stacked) C planes. It was also necessary to make rather arbitrary assumptions for the inelastic electron mean free path l, and for the EXAFS Debye-Waller factor. For the mean free path, we chose an energy-independent value of 7 Å. With this choice we also obtain $e^{-2r_{NN}/l}$ ~ 0.35—0.4, not an unusual factor to obtain between Lee-Beni theory and experiment where r_{NN} corresponds to the nearest-neighbor Br-C interatomic distance. The

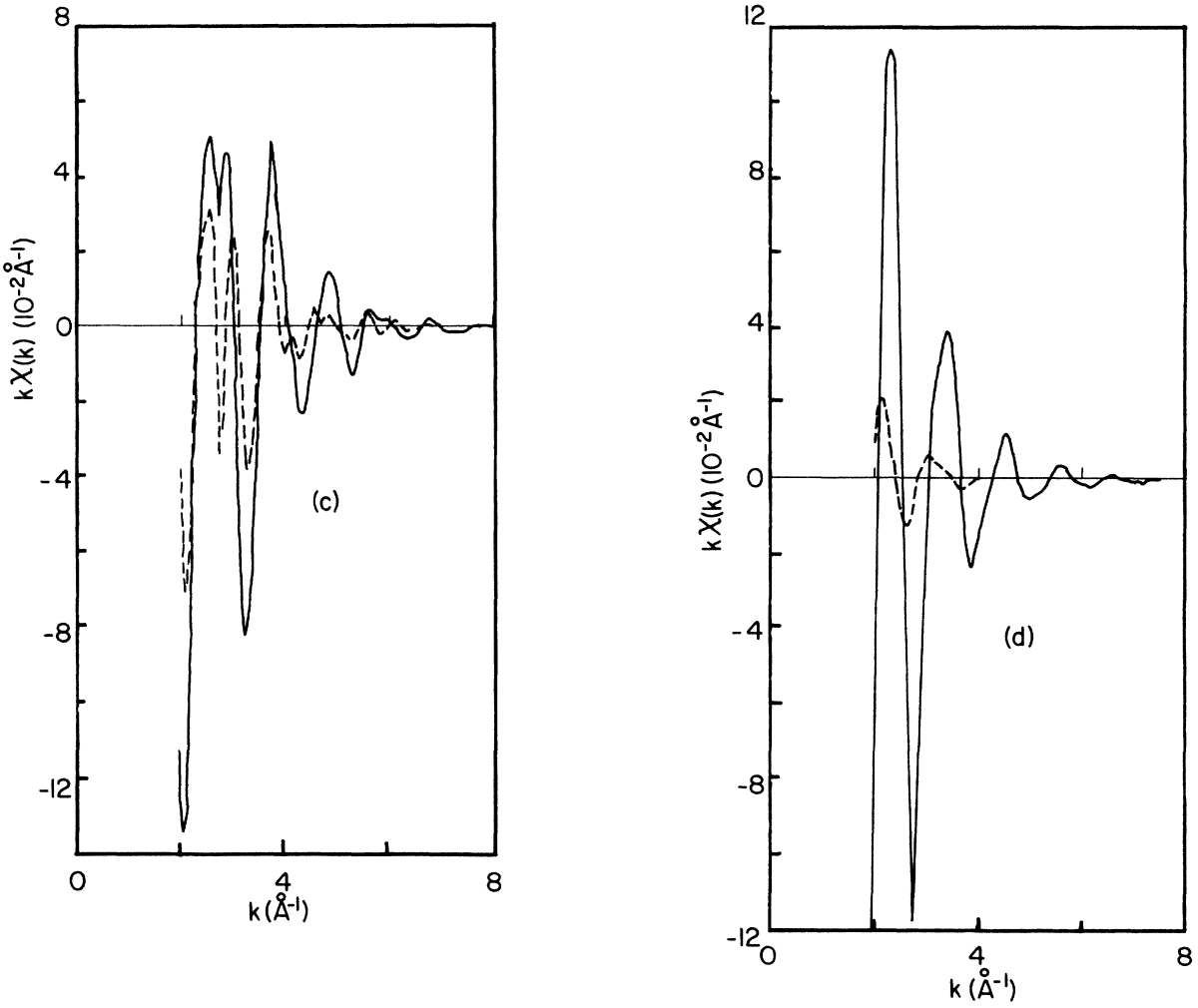

FIG. 21. Continued.

EXAFS Debye-Waller factor was assumed to be independent of the particular Br-C distance (we simply chose $\sigma=0.156$ Å which is an estimated value of the root-mean-square Br-atomic displacement from the x-ray-diffraction results of Ref. 26).

Our results are shown in Fig. 21. Figure 21(a) is based on the GC model where all Br sites are assumed to be in the plane midway between graphite planes. Figure 21(b) is also based on the GC in-plane model but certain nearest-neighbor pairs (1-1′ of Fig. 2 of Ref. 24) are tilted out of the plane by an angle of 13°. Upon comparing Figs. 21(a) and 21(b) we observe a marked "out-of-plane" effect on Br-C EXAFS. Figure 21(c) is based on the ET (Fig. 10 of Ref. 27) in-plane Br sites with 14° and 23° out-of-plane tilts of the two uniquely different nearest-neighbor pairs within the ET unit cell. We note that these latter tilt angles were chosen to yield a single Br-Br nearest-neighbor distance of 2.31 Å. Finally, Fig. 21(d) gives results for our uniform distribution in-plane model. It is noteworthy that we obtain a sizeable EXAFS signal in 45° orientation for this model. The results resemble a single-shell signal, although clearly many Br-C distances contribute. Also, as can be seen by comparing Figs. 17 and 21(d), excellent agreement with experiment (based on $E_0=9.75$ eV) is found in the case of 45° orientation, although the anisotropy does not appear to be correctly given by the model as the model gives a signal in parallel orientation which is too small. Next consider the difference in results for $k\chi(k)$ in 45° orientation between the GC in-plane model [Fig. 21(a)] and the uniform distribution model [Fig. 21(d)]. Clearly the major effect in $k\chi(k)$ of uniformly distributing the sites is to greatly decrease the amplitude. From our previous discussion of experimental results it therefore appears that this model of disordering mimics the melting transition reasonably well.

None of the above models yield satisfactory agreement with room temperature experimental results, although certain features of the data can be seen to be well represented by each of the models. The comparison with experiment is also confused by the uncertainty in extracted Br-C EXAFS for parallel orientation. However, it is of interest that certain other models, which are inconsistent with x-ray diffraction results, do *not* improve the Br-C EXAFS results. In particular, we have considered "single-site" models, with sites in the plane midway between the adjacent graphite planes. The planar components of the Br

sites were chosen to correspond to the following positions with respect to the adjacent carbon planes: carbon sites, midpoints of nearest-neighbor carbon separations, and carbon hexagon centers. Of these latter models the first is most clearly inappropriate since it yields an EXAFS signal which is as great for parallel orientation as for 45° orientation, in obvious disagreement with experiment.

X. NON-GAUSSIAN EFFECTS

One can merely speculate, at present, about the physical significance of the discrepancies found among Br-Br EXAFS amplitudes and phases, i.e., E_0 values. We believe that the most likely possibilities are electronic effects (such as inelastic-electronic mean-free-path differences among Br compounds and Br_2 vapor), and non-Gaussian Debye-Waller effects. Both of these effects could possibly explain both the amplitude and the (less pronounced) phase discrepancies we observed. However, it is noted that there does not appear to be a simple correlation between amplitude and phase effects as our two HOPG samples, which yield differing amplitudes by $\sim 20\%$, also appear to yield identical phases. Other possible explanations for a decrease in Br-Br EXAFS amplitude from that expected on the basis of Br_2 vapor results are (a) that a significant fraction of bromine is present which is chemically in atomic form, (b) sample thickness or hole effects, or other possible experimental effects, and (c) an impurity effect. These latter explanations are not as likely to be correct, however, in view of the full spectral information obtained and the numerous checks (see Sec. V) we have made on our results. In order to explain our *EXAFS* results on the basis of (a) for example, it would then also appear necessary to postulate that, of the atomic Br, the Br $4p$ atomic-like states are split by the crystal field such that there is fortuitously little or no difference in *anisotropy* between the Br-Br EXAFS amplitude and the WL peak height, and further that those states indeed yield nearly the same WL peak height as does a Br_2 antibonding state. Here, it is presumed that the nonatomic bromine is Br_2. Further, we have found that Br-C EXAFS is quite sensitive to the Br sites, so the sizeable difference in Br-Br EXAFS between our two HOPG samples accompanied by virtually identical 45° Br-C EXAFS signals is also a surprising result given explanation (a), which would presumably require differing Br sites between our HOPG samples. Explanation (c) would require the presence of impurity bonds with Br, of a concentration about 30 at.% of the Br concentration, which amounts to about a 1–2 *overall* impurity atomic percentage. It would further require that each of those bonds yield approximately the same white-line contribution as does each of the Br_2 bonds, that their orientations be approximately the same (with respect to the graphite planes) as those of the Br_2 bonds and, of course, that they do not have a signal in the Br-Br EXAFS regime. Here, as in our discussion of (a), it is *presumed* that the bromine is predominantly Br_2.

Next we examine whether our Br-Br EXAFS data can be explained in terms of non-Gaussian Debye-Waller factor effects in Br-graphite with the presumption that the bromine is in the form of essentially Br_2 molecules. The structurally dependent single-shell EXAFS-amplitude factor is written as

$$(1/r^2)e^{-2k^2\sigma^2+Bk^4}$$

in the usual leading-term (in a cumulant expansion) non-Gaussian approximation. We wish to explain the *decreased* amplitude in our Br-graphite materials through this factor. Upon choosing r of Br-graphite to be 2.36 Å for this purpose, we wish to see if our data can be made to satisfy

$$\frac{A_{\text{vap}}(k)}{A_{\text{Br-G}}(k)} = 1.07\exp[-2k^2(\sigma^2_{\text{vap}}-\sigma^2_{\text{Br-G}})-B_{\text{Br-G}}k^4]\,, \tag{2}$$

where $A(k)$ is defined as the measured EXAFS amplitude (for graphite compounds denoted here as Br-G, a spherical average is used). Note that the largest possible value of r for Br graphite yields the best chance of successfully fitting the amplitudes, and we will see that 2.36 Å is consistent with the EXAFS phases. We determine $\Delta\sigma^2 \equiv \sigma^2_{\text{vap}} - \sigma^2_{\text{Br-G}}$ and $B_{\text{Br-G}}$ by fitting to experiment at two widely spaced values of k. The result is $\Delta\sigma^2 = -4.0\times10^{-3}$ Å^2 and $B_{\text{Br-G}} = 2.1\times10^{-5}$ Å^4 for HOPGl; the overall agreement with experiment is seen (Fig. 22) to be poor. Similarly upon comparing room-temperature data in parallel orientation for HOPGl and HOPGv it is found that $\sigma^2_{\text{HOPG}v} - \sigma^2_{\text{HOPG}l} = 2.3\times10^{-3}$ Å^2 and $B_{\text{HOPG}v} - B_{\text{HOPG}l} = 1.7\times10^{-5}$ Å^{-4}. (The ratio of r^2 values is taken as unity.) These latter data are compared in Fig. 23 on the basis of this analysis; the fit is seen to yield agreement with experiment. Therefore, for this latter amplitude discrepancy, a leading-term non-Gaussian—Debye-Waller-factor explanation is possible.

A similar non-Gaussian—Debye-Waller-factor-type

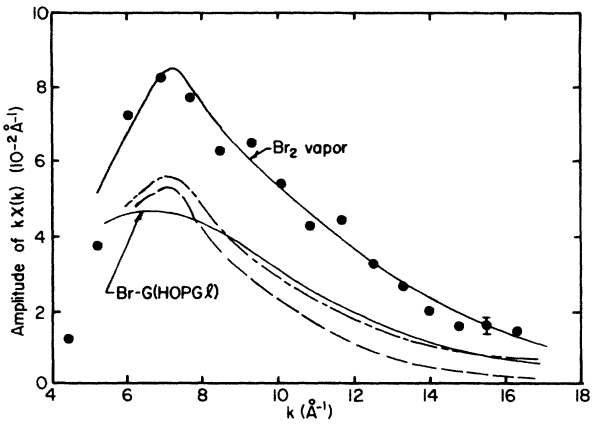

FIG. 22. Comparison between the Br-Br EXAFS amplitude of Br_2 vapor and HOPGl. Solid circles represent peaks and troughs of $k\chi(k)$ in the case of Br_2 vapor and solid curves are drawn through those data (not shown for HOPGl) for both Br_2 vapor and HOPGl. The curve representing HOPGl data corresponds to a spherically averaged $\chi(k)$, or $\frac{2}{3}\chi_{45°}+\frac{1}{3}\chi_{11}$. Dashed and dashed-dotted curves represent the Br_2-vapor-amplitude function multiplied, respectively, by Gaussian and non-Gaussian Debye-Waller factors (see text).

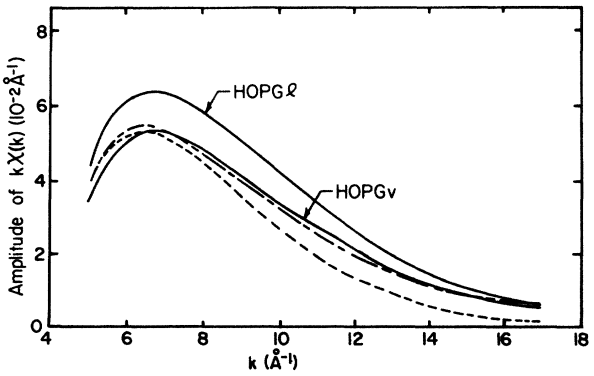

FIG. 23. Comparison between the Br-Br EXAFS amplitudes of HOPG l and (room temperature) HOPG v. Solid lines are hand-drawn through peak and trough heights of parallel orientational data. Dashed and dashed-dotted curves correspond, respectively, to the results for HOPG l multiplied by Gaussian and non-Gaussian Debye-Waller factors (see text).

analysis of the apparent shift in E_0 between Br_2 vapor and Br-graphite is made in Fig. 24. It is presumed that there exists a k^3 contribution to the phase function[30] which gives rise to the apparent E_0 shift. The straight lines in the figure are in accord with this presumption. It is also assumed that the "experimental" phase for each material is given by the previously fitted Lee *et al.* function of this work. Crude estimates of the experimental uncertainties in the phase are shown, and on this basis we see that the data can indeed be discussed in terms of a single value of E_0, but where the intramolecular distance of Br graphite is 2.34—2.36 Å. Indeed, fits to the data using the derived phase-function parameters of Fig. 24 verify these conclusions.

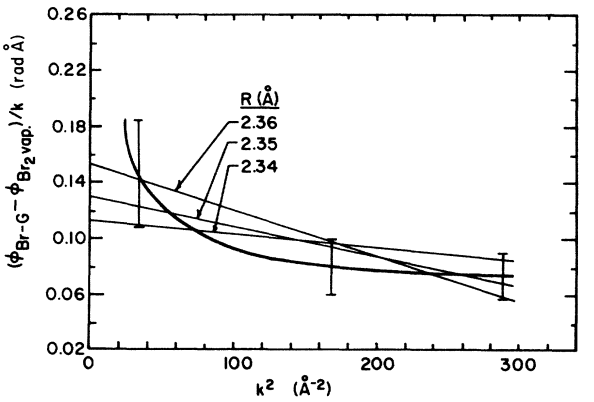

FIG. 24. Comparison between Br-Br EXAFS phase functions of Br-graphite and Br_2 vapor. The difference in phase functions is based on least-square fits, with different E_0 values, within the Gaussian Debye-Waller approximation. The error bars are crude estimates obtained from results for $k\chi(k)$. The straight lines correspond to the assumption of the same E_0 value for both Br-graphite and Br_2 vapor, and the inclusion of a k^3, or non-Gaussian, term in the Br-graphite phase function. Corresponding values of the nearest-neighbor Br distance are indicated.

XI. COMPARISON WITH ADSORBED RESULTS

It is possible to make a comparison of our data to the $T=105$ K data of Heald and Stern[4] on adsorbed Grafoil, although it should be noted that the latter measurements yielded puzzling temperature dependences of EXAFS amplitudes between $T=105$ K and room temperature. Apparently their results for $\chi(k)$ are based on an E_0 value of 7 eV, so we show both their results and ours, using $E_0=7$ eV, in Figs. 25 and 26. Only our room temperature HOPG v results are shown. There exists agreement (between these intercalated and adsorbed data) in the positions of the peaks between corresponding orientational data and also agreement in the Br-Br parallel-orientational EXAFS amplitudes. It should be noted that for the purposes of making this comparison we formed $\mu_\perp = 2\mu_{45°} - \mu_{||}$ in the case of the HOPG v results. Interestingly, corresponding to $\mu_\perp$, and at low k, the intercalated amplitudes are approximately twice the adsorbed ones which is just what one would expect assuming that the Br's occupy the same (two-dimensional) sites in the two systems and assuming a Br-C EXAFS picture. It also appears, from a careful comparison of the Br-Br EXAFS, shown in Figs. 25 and 26, that there may exist a slight increase in intramolecular distance, perhaps from 2.31 to 2.34 Å, as previously suggested by Heald and Stern, in going from adsorbed to intercalated materials.

Finally, the fact that a slight qualitative difference in signal in the very-low-energy region, and in parallel orien-

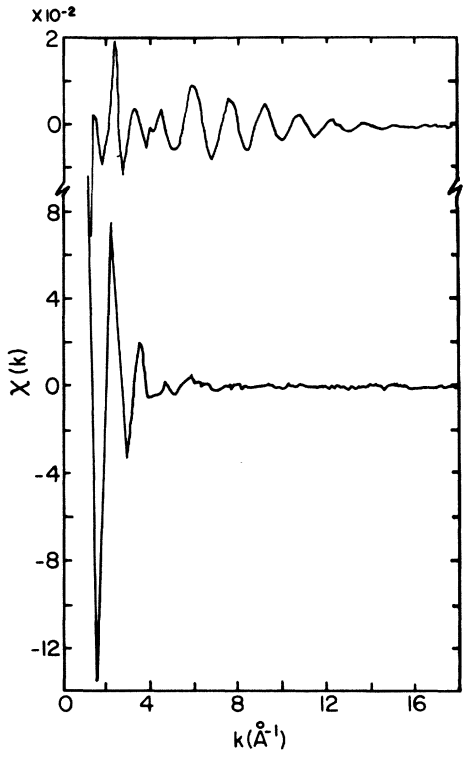

FIG. 25. $\chi(k)$ of HOPG v at room temperature. Results are based on $E_0=7$ eV. Upper curve is directly obtained from data in parallel orientation. Lower curve, corresponding to perpendicular orientation, is indirectly obtained through the expression $\mu_\perp = 2\mu_{45°} - \mu_{||}$.

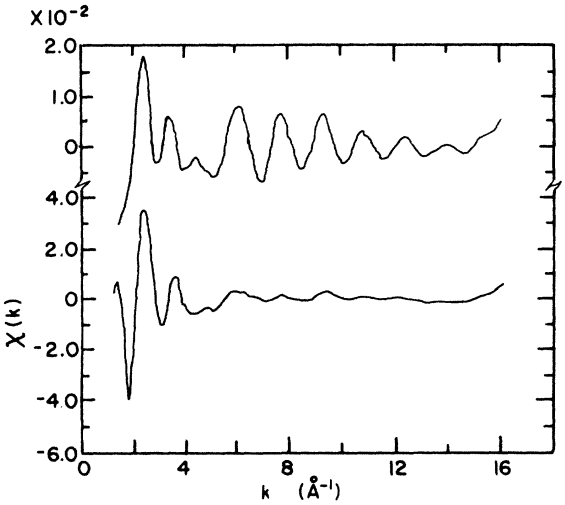

FIG. 26. Results of Ref. 4 for $\chi(k)$ of Br adsorbed Grafoil at $T=105$ K. Upper and lower curves are directly obtained from data in parallel and perpendicular orientations, respectively.

tation, is noticeable between adsorbed and intercalated materials might be related to the different monochromating conditions used in the two experiments; Heald and Stern used the Si(111) reflection which yields a somewhat less resolved beam than does the Si(220) reflection, which we used.

XII. SUMMARY AND CONCLUSION

We performed linearly polarized Br K-edge EXAFS measurements on several desorbed GIC-Br samples, HOPG and fiber-based, as well as on Br_2 vapor. Br-Br EXAFS as well as white-line-intensity results, as a function of sample orientation with respect to the x-ray polarization, yielded an effective angle of $\alpha=16\pm4°$ of nearest-neighbor Br bonds with respect to the neighboring graphite planes; we could observe no clear change in the value of α among samples and temperatures studied.

We have also observed several sample and thermal effects, identified a contribution of further-than-nearest-neighbor Br-Br distances to the EXAFS signal, and provided an improved analysis of Br_2 vapor EXAFS. The temperature-dependent effects (although our measurements are sparse in this regard) have been discussed in terms of known structural transitions from diffraction data for HOPG and single-crystal-based materials. We suggest, on the basis of our results, that, unlike HOPG-based materials, fiber-based materials have no intercalate two-dimensional order down to 300 K. We have also shown, through our ability to render several possibilities implausible, that a discrepancy in Br-Br EXAFS amplitude between Br_2 vapor and Br-graphite is most likely an electronic effect. However, this discrepancy in addition to a similar sample preparation effect in the Br-Br EXAFS amplitude are largely unexplained.

Finally, simplified model calculations of Br-C EXAFS in Br-graphite have also been presented. These calculations show, somewhat surprisingly, that a sizeable signal in 45° orientation (of the x-ray polarization with respect to the graphite planes in HOPG) is expected for a uniform two-dimensional distribution model for the Br sites and that the k dependence of that signal is quite similar to what we observed. On the other hand, that structural model predicts a quite small signal in parallel orientation, seemingly in disagreement with our observations. Other models considered are those based on commensurate phase in-plane structures as obtained from previous interpretations of x-ray-diffraction measurements. Out-of-plane components, approximately consistent with the other results of this work, were also included in our models. Thus, the effects of different intercalate structural models on Br-C EXAFS were briefly studied. It appears that commensurate models yield improved results, in comparison to those of the uniform distribution model, for the relative strengths of Br-C EXAFS signals in parallel and 45° orientation.

ACKNOWLEDGMENTS

The work reported herein was (partially) done at Stanford Synchrotron Radiation Laboratory (SSRL), which is supported by the U.S. Department of Energy (Basic Energy Sciences Program), by The National Science Foundation (Division of Materials Research), and by the National Institute of Health (Biotechnology Resource Program, Division of Research Resources). We wish to thank Dr. S. B. Qadri and Dr. D. J. Nagel for helpful conversations during the course of this work. We also thank Mr. N. Chen for his assistance in a portion of the data analysis and the staff of the SSRL for their technical assistance.

APPENDIX: Br-Br EXAFS PARAMETRIZATION

Neither the Teo *et al.* fits nor the actual theoretical results for the amplitude agree with experiment (Fig. 3) for $k\leq5$ Å^{-1}. Since the calculated amplitude function has a peak at $k\approx3.6$ Å^{-1} in addition to the one at 8.6 Å, we decided to fit the experimental results to the empirical formula

$$F=(1-Q)F_1+QF_2\ ,$$

where $Q=(k-4.25)/(6-4.25)$ for $4.25\leq k\leq6$ Å^{-1}, $Q=1$ for $k>6$ Å^{-1}, and $Q=0$ for $k<4.25$ Å^{-1}. Here F_1 and F_2 are Lorentzian functions: F_2 is given by the Teo *et al.* (expt.) parameters except for the scale factor A determined from a fit to experiment in the region $6\leq k\leq17$ Å^{-1}: F_1 is determined from a fit to theory *and* experiment at low k; the breadth and peak position of the Lorentzian F_1 were estimated by roughly fitting the theoretical results given in Fig. 4 of Ref. 19 and the peak height was determined from experiment. We note that Lee and Beni presented results of calculations of the amplitude and phase functions for $2.8\leq k\leq15.1$ Å^{-1}. Furthermore, it is stated in the Lee *et al.* paper that the fits to the theoretical phases are for the range 4 Å$^{-1}\leq k\leq16$ Å^{-1}. (Presumably this is the case for the amplitude parametrization as well.)

TABLE VI. Br-Br EXAFS amplitude for Br_2 vapor: parametrization. Value in parentheses represents fit to Lee-Beni theory. Units: A_1, A_2, B_1, B_2 (Å); C_1,C_2 (Å^{-1}).

k-range (Å^{-1})	Functional form	This work[a]	Parameters Teo *et al.* (expt.)	Parameters Teo *et al.* (theor.)
$2<k<4.25$	$F_1=\frac{A_1}{1+B_1^2(k-C_1)^2}$	$A_1=0.079(0.41)$		
		$B_1=0.85$		
		$C_1=3.6$		
$6<k<16$	$F_2=\frac{A_2}{1+B_2^2(k-C_2)^2}$	$A_2=0.465$	0.36	0.59
		$B_2=0.181$	0.181	0.1617
		$C_2=8.57$	8.57	8.764
$4.25<k<6$	$F=QF_1+(1-Q)F_2$	$Q=\frac{k-4.25}{1.75}$	$Q=0$	$Q=0$

[a]For $k\geq 6$ we simply adopted the Teo *et al.* (expt.) values for B and C rather than obtain them through least-square procedures. Results are shown in Fig. 3.

We adopted the theoretical phase function for $k\geq 2.8$ Å^{-1}, but since the Lee *et al.* fit can be seen to be somewhat inaccurate in the region of the peak in $\phi(k)$ (at $k=5$ Å^{-1}) we included the correction term $e^{-2.85(k-5)^4}$ rad in the Lee *et al.* formula. Also the Lee *et al.* fit does not represent the theory very well for $k<4$ Å^{-1}. Therefore we used a quadratic expression for $k<4.2$ Å^{-1} with parameters fit to the calculated values, and, for $k<2.8$ Å^{-1}, ϕ was assumed to be constant.

It is worthwhile to compare the Teo *et al.*[15] parametrizations, the Lee and Beni[19] amplitude results, and experiment in more detail. The Teo *et al.* fits of the amplitude use the Lorentzian $A/[1+B^2(k-C)^2]$. Two sets of parameters were given, one based on a fit to the theoretical results of Lee and Beni and the other based on a fit to experiment (Kincaid and Eisenberger[18]), where the experimental data were normalized by a different procedure than that used here. For fixed A both sets of parameters B and C give results to within a few percent of each other between $k=6$ and $k=8$ Å^{-1}. However, below $k=8$ Å^{-1} the fit, with the "theoretical" A of 0.59 Å^{-1}, yields poor agreement with the Lee and Beni results; at $k=6$ Å^{-1} it overestimates the Lee-Beni result by $\sim 25\%$. One of the results of the fits of our experimental data to the Teo *et al.*—Lee *et al.* formulas was a value for A which is in the ratio of 0.8 ± 0.02 to the theoretical value. Furthermore, the fit to the data appears to be good at $k=6$ Å^{-1} and at $k>8$ Å^{-1}. (These parametrizations are summarized and compared with theoretical results in Table VI.) The magnitude of the trough at $k\approx 7$ Å^{-1}, however, is underestimated by the fit shown in Fig. 3 by approximately 20%.

[1]J. L. Feldman, E. F. Skelton, A. C. Ehrlich, D. D. Dominguez, W. T. Elam, S. B. Qadri, and F. W. Lytle, Solid State Commun. **49**, 1023 (1984).

[2]J. L. Feldman, W. T. Elam, A. C. Ehrlich, E. F. Skelton, D. D. Dominguez, S. B. Qadri, D. D. L. Chung, and F. W. Lytle, in *EXAFS and Near Edge Structure III,* edited by K. O. Hodgson, B. Hedman, and J. E. Penner-Hahn (Springer-Verlag, Berlin, 1984), p. 464.

[3]K. K. Bardhan, J. C. Wu, and D. D. L. Chung, Synth. Met. **2**, 109 (1980); D. D. L. Chung, J. Electron. Mat. **7**, 89 (1978).

[4]S. M. Heald and E. A. Stern, Phys. Rev. B **17**, 4069 (1978); Synth. Met. **2**, 87 (1980).

[5]A. Erbil, A. R. Kortan, R. J. Birgeneau, and M. S. Dresselhaus, Phys. Rev. B **28**, 6329 (1983).

[6]D. Ghosh and D. D. L. Chung, Mater. Lett. **3**, 161 (1985).

[7]D. Ghosh and D. D. L. Chung, J. Phys. Lett. **44**, 761 (1983).

[8]D. Ghosh and D. D. L. Chung, Mater. Res. Soc. Symp. Proc. **20**, 15 (1983).

[9]D. Ghosh and D. D. L. Chung, Mat. Res. Bull. **18**, 1179 (1983).

[10]R. Al-Jishi and G. Dresselhaus, Mat. Res. Soc. Symp. Proc. **20**, 301 (1983).

[11]A. Erbil, G. Dresselhaus, and M. S. Dresselhaus, Phys. Rev. B **25**, 5451 (1982).

[12]H. Morawitz, P. Bagus, T. Clarke, W. Gill, P. Grant, G. B. Street, and D. Sayers, Synth. Met. **1**, 267 (1980).

[13]H. Oyanagi, M. Tokumoto, T. Ishiguro, H. Shirakawa, H. Nemoto, T. Matsushita, M. Ito, and H. Kuroda, J. Phys. Soc. Jpn. **53**, 4044 (1984); W. Krone, G. Wortmana, K. H. Frank, G. Kaindl, K. Menke, and S. Roth, in *EXAFS and Near Edge Structure III,* edited by K. O. Hodgson, B. Hedman, and J. E. Penner-Hahn (Springer-Verlag, Berlin, 1984), p. 394.

[14]D. Ghosh, R. Gangwar, and D. D. L. Chung, Carbon **22**, 325 (1984).

[15]B. K. Teo, P. A. Lee, A. L. Simons, P. Eisenberger, and B. M. Kincaid, J. Am. Chem. Soc. **99**, 3854 (1977).

[16]P. A. Lee, B. K. Teo, and A. L. Simons, J. Am. Chem. Soc. **99**, 3856 (1977).

[17]E. A. Stern, S. M. Heald, and B. Bunker, Phys. Rev. Lett. **42**, 1372 (1979).

[18]B. M. Kincaid and P. Eisenberger, Phys. Rev. Lett. **34**, 1361 (1975).

[19]P. A. Lee and G. Beni, Phys. Rev. B **15**, 2862 (1977).

[20]J. J. Rehr and S.-H. Chou, in *EXAFS and Near Edge Structure,* edited by A. Bianconi, L. Incoccia, and S. Stipcich (Springer-Verlag, Berlin, 1983), p. 22.

[21]P. Lagarde, Phys. Rev. B **14**, 741 (1976).

[22]J. L. Dehmer and D. Dill, J. Chem. Phys. **65**, 5327 (1977).

[23]This equality is probably valid within the shape-resonance interpretation as well: See D. Dill, J. Siegel, and J. L. Dehmer, J. Chem. Phys. **65**, 3158 (1976).

[24]S. M. Heald, in *EXAFS and Near Edge Structure* (Ref. 20), p. 98.

[25]W. Ekardt and D. B. Tran Thoai, Solid State Commun. **40**, 939 (1981).

[26]D. Ghosh and D. D. L. Chung, Synth. Met. **7**, 283 (1983).

[27]W. T. Eeles and J. A. Turnbull, Proc. Phys. Soc. London, Sect. A **283**, 179 (1965).

[28]We used the results of Refs. 15, 16, and 19, and of Kincaid [B. M. Kincaid, Stanford Synchrotron Radiation Project Report No. 75/03, 1975 (unpublished)], as well as a slight extrapolation of the phase function at low k.

[29]T. Sasa, Y. Takahashi, and T. Mukaibo, Carbon **9**, 407 (1971); S. Y. Leung, M. S. Dresselhaus, C. Underhill, T. Krapchev, G. Dresselhaus, and B. J. Wuensch, Phys. Rev. B **24**, 3505 (1981).

[30]P. Eisenberger and G. S. Brown, Solid State Commun. **29**, 491 (1979).